IEEE Access
Multidisciplinary | Rapid Review | Open Access Journal

Received August 5, 2021, accepted August 16, 2021, date of publication August 20, 2021, date of current version August 27, 2021.

Digital Object Identifier 10.1109/ACCESS.2021.3106448

Optimal Model Predictive and Linear Quadratic Gaussian Control for Frequency Stability of Power Systems Considering Wind Energy

MOHAMED KHAMIES[1], GABER MAGDY[2], SALAH KAMEL[1], AND BASEEM KHAN[3], (Member, IEEE)

[1]Electrical Engineering Department, Faculty of Engineering, Aswan University, Aswan 81542, Egypt
[2]Department of Electrical Engineering, Faculty of Energy Engineering, Aswan University, Aswan 81528, Egypt
[3]Department of Electrical and Computer Engineering, Hawassa University, Hawassa 1530, Ethiopia

Corresponding authors: Gaber Magdy (gabermagdy@aswu.edu.eg), Salah Kamel (skamel@aswu.edu.eg), and Baseem Khan (baseem.khan04@gmail.com)

This work was supported by the National Research and Development Agency of Chile (ANID) under Grant ANID/Fondap/15110019.

ABSTRACT This work presents a new robust control technique which combines a model predictive control (MPC) and linear quadratic gaussian (LQG) approach to support the frequency stability of modern power systems. Moreover, the constraints of the proposed robust controller (MPC-LQG) are fine-tuned based on a new technique titled Chimp optimization algorithm (ChOA). The effectiveness of the proposed robust controller is tested and verified through a multi-area power system (i.e., single-area and two-area power systems). Each area contains a thermal power plant as a conventional generation source considering physical constraints (i.e. generation rate constraint, and governor dead band) in addition to a wind power plant as a renewable resource. The superiority of the proposed robust controller is confirmed by contrasting its performance to that of other controllers which were used in load frequency control studies (e.g., conventional integral and MPC). Also, the ChOA's ingenuity is verified over several other powerful optimization techniques; particle swarm optimization, gray wolf optimization, and ant lion optimizer). The simulation outcomes reveal the effectiveness as well as the robustness of the proposed MPC-LQG controller based on the ChOA under different operating conditions considering different load disturbances and several penetration levels of the wind power.

INDEX TERMS Frequency control (LFC), model predictive control (MPC), linear quadratic gaussian (LQG), wind energy, chimp optimization algorithm.

NOMENCLATURES

WPGS	Wind power generating system
RESs	Renewable energy sources
LFC	Load frequency control
ANN	Artificial neural networks
LQG	Linear quadratic Gaussian
LQR	Linear quadratic regulator
PID	Proportional-integral-derivative
MPC	Model predictive control
GRC	Generation rate constraint
GDB	Governor dead band
HVDC	High voltage direct current
ChOA	Chimp optimization algorithm
ITAE	Integral time-weighted absolute error
PSO	particle swarm optimization
GWO	gray wolf optimization
ALO	ant lion optimizer
X	The state vector
Y	The control output vector
U	The control input signal
W	The disturbance vector
B	The control output vector
E	The disturbance input
C	A variable relates to output measurement
$\mathbf{\Delta P_G}$	The change of the governor output (MW pu)
$\mathbf{\Delta P_m}$	The change of mechanical power (MW pu)
$\mathbf{\Delta f}$	The frequency deviation (MW pu)

The associate editor coordinating the review of this manuscript and approving it for publication was Mauro Gaggero.

This work is licensed under a Creative Commons Attribution 4.0 License. For more information, see https://creativecommons.org/licenses/by/4.0/

ΔP_L	The change of load (MW pu)
ΔP_c	The regulating system frequency (MW pu).
H	The inertia constant *(pu.MW s)*
D	The coefficient of equivalent damping *(pu MW /HZ)*
R	The regulation of governor speed *(Hz/pu.MW)*
T_g	The time constants of the governor *(sec)*
T_t	The time constants of a turbine *(sec)*
ΔP_{wind}	The wind power variation
ΔP_{WT}	The wind turbine output power
ρ	Air density (kg/m^3)
A_T	Area of the rotor swept (m^2)
V_W	The rated wind speed (m/s)
C_P	Power coefficient of the rotor blades
$C_1 - C_7$	The turbine coefficients
β	The pitch angle
r_T	The radius of rotor (m)
λ_T	Tip-speed ratio (TSR)
λ_I	An intermittent TSR
Q_{LQG}	Weight input matrix
R_{LQG}	Control input matrix
S_0	A diagonal matrix of output scale factors
x_p	The system state vector
u (k)	The vector with manipulated control output
d (k)	The vector with unmeasured disturbance
v (k)	The vector with measured disturbances
B_{pu}, B_{pv}, *and* B_{pd}	The corresponding columns of B
D_{pu}, D_{pv}, *and* D_{pd}	The corresponding columns of D
w_d (k)	The dimensionless noise inputs
x_d (k)	The input disturbance model states
A_d, B_d, C_d *and* D_d	The constant state-space matrices
A_n, B_n, C_n *and* D_n	The constant state-space matrices
x_n (k)	The vector of the noise model state
y_n (k)	The vector of noise signals
w_n (k)	The vector dimensionless of the noise input
J	The quadratic cost function
t_{sim}	The simulation time
k_l	The linear gain of the LQG controller.
k_q	The quadratic gain of the LQG controller
k_r	The regulator gain of the LQG controller
L	The Kalman gain
t_i	iteration of the current number
X_{prey}	the position vector of the predator
X_{chimp}	the vector of chimp position
a, d, *and* m	the coefficient vectors
r_1 and r_2	the unsystematic vectors
m	a chaotic vector
T	the cumulative number of iterations
μ	a random number that relies on between 0 and 1
t_s	The sampling time
P	The prediction horizon
M	The control horizon
W	The weight of the MPC controller
Q_{MPC} and R_{MPC}	The weight factors of the MPC controller
P	The symmetric positive matrix

I. INTRODUCTION

Recently, significant efforts have been developed for increasing the share of renewable energy sources (RESs) into power grids to reduce the problems arising from fossil fuel problems associated with traditional power plants [1]. However, the RESs penetration has an appreciable influence on the operation as well as stability of the power system due to its effect in reducing the system's inertia. As a result, as the interpenetrating level of RESs grows, the system frequency fluctuates much more, and hence the reliability of the system is severely affected [2], [3]. In addition, the high demand for human activities in consuming high electricity than the considered generation increases the instability problem. Furthermore, these instability problems affect the operation of the system and security. Therefore, it is necessary to avoid any reasons that lead to deviations in the system frequency/voltage to preserve the reliability and security of the system. From all possible solutions, load frequency control (LFC) is regarded as the best solution to eliminate the frequency and tie-line power deviations in interconnected systems, thus return the system to its normal operation [4].

A. LITERATURE REVIEW

Many studies have been carried out to actualize the system's frequency stability in abnormal conditions and to sustain system stability in normal conditions. In this regard, different control procedures have been implemented in the power system to fulfill their roles in ensuring the stability of the system. Therefore, some researchers applied robust control techniques (e.g., H_infinite controller [5], coefficient diagram method [6], μ-synthesis [7], H2 / H∞ approach [8], and so on) to support the power system frequency stability taking into account RESs. Moreover, numerous intelligent control techniques (e.g. fuzzy logic control [9], fuzzy-proportional integral (PI) controller [10], the adaptive neuro-fuzzy logic controller [11], artificial neural networks (ANN) [12], layered recurrent ANN [13]) have been implemented to regulate the system frequency. Also, several digital control techniques have been implemented for frequency regulation of power systems in [14], [15]. Furthermore, optimal control techniques such as; linear quadratic regulator (LQR) [16] and linear quadratic Gaussian (LQG) [17], have been applied for enhancing the frequency stability of the

system. On the other hand, researchers have preferred to use the proportional-integral-derivative (PID) controller owing to its advantages (i.e. simplicity and requiring less cost). However, the PID controller gives an undesired performance in abnormal operating conditions due to its high sensitivity. As a result, an optimal PID controller must be designed [18]. Therefore, traditional optimization methods such as; tracking approach [19], aggregation methods [20], and interior-point algorithm [21] have been applied to adjust the constraints of the PID controller. Furthermore, heuristic and meta-heuristic optimization methods have been recently applied in solving different optimization problems including determining the optimum constraints of the frequency controller. In the following, different meta-heuristic optimization methods were used for determining PI/PID controller parameters such as; slap swarm algorithm [22], lightning attachment procedure optimization [4], moth swarm optimization [23], and imperialist competitive algorithm [24].

Also, a new predictive functional modified PID has been established to keep the system performance stable during system uncertainties [25].

Furthermore, a novel variable structure gain scheduling has been proposed to allow rapid switching between two considered PI controllers in order to improve system stability [26] Furthermore, different studies applied fractional-order controllers due to their extra flexibility and robustness in the control process [27]. On the other side, some researchers prompted more interest to apply the model predictive control (MPC) due to its merits (i.e. easy implementation, flexibility, handle with system nonlinearities, and fast response) [2]. Therefore, the MPC strategy has been effectively applied to improve the frequency performance in several LFC studies [2], [24]–[33]. In this regard, a distributed MPC has been applied for supporting the multi-area power grid stability while taking the generation rate constraint (GRC) into account [28]. Also, the MPC strategy has been employed for improving the single-area power system performance seeing the GRC as well as governor dead band (GDB) [29]. Additionally, a decentralized MPC has been implemented in a multi-source power grid to enhance the stability of the system's frequency considering uncertainties as well as nonlinear effects [30]. Furthermore, the MPC strategy has been applied in the real power grid, which includes both traditional generation sources as well as wind turbines, for boosting the system stability seeing an inherent nonlinearity [31]. Also, the LFC based on the MPC strategy has been implemented in a multi-area hybrid power grid seeing the penetration effect of the wind power [32]. In [33], MPC has been applied to the multi-area power grid, where each controller for each area is configured separately for ensuring the stability of the system. Furthermore, the MPC has been applied to enhance the frequency deviations considering renewables penetration and integration of energy storage devices [34]. Also, the adaptive MPC (AMPC) has been applied to a single-area power system considering integration of wind turbines, and system nonlinearities for improving the system performance [35]. As well, the MPC has been applied to the demand and supply sides for optimal power tracking control [36]. Furthermore, MPC has been applied for a grid combining new power generation sources, and energy storage units [37]. Additionally, the MPC has been applied to a grid to control a wind turbine system [38]. Also, many efforts and endeavors have been made to adjust optimal parameters of MPC based on different optimization techniques. For example, Bat inspired algorithm (BIA) was used to determine the optimal constraints of the MPC for the LFC of (thermal–hydro) interconnected power grid where the system performance-based an optimal MPC has been compared the system performance-based PI controller [39]. As well, the gravitational search algorithm was applied to select the optimal parameters of MPC to reduce the frequency fluctuation for the LFC study considering three different area power systems [40]. Also, in a wind energy conversion system, the crow search algorithm has been applied to select the optimal parameters of the AMPC for blad batch control [41]. In addition, a recent sooty turn algorithm has been applied to select MPC parameters where the superconducting magnetic energy storage was considered for enhancing the performance of the considered system based on the secondary control loop [42]. Also, the constriction coefficient particle swarm optimization has been applied to adaptive MPC to keep the system stability under the renewable sources penetration [2].

Recently, to improve the system performance-based LFC, supplementary control techniques (e.g., LQR, and LQG) have been introduced. For example, in a three-area power grid with high voltage direct current (HVDC) transmission lines, the LQR technique has been linked with the Kalman filter for improving system performance [43]. Moreover, the LQR has been applied with the PID controller for boosting the performance of the smart grid comprising wind turbines [16]. On the other side, the LQG technique is attached with the integral gain for diminishing any oscillations in frequency response in an integrated power grid. Besides, this strategy gives better performance than using the LQG controller alone [17]. However, different studies considered different optimization techniques to determine the optimum constraints of the LQR, and LQG [4], [44].

In recent years, the ChOA algorithm was proposed by Khishe and Mosavi to solve the optimization problems of several engineering applications [45]. Where the proposed ChOA algorithm mimics the chimp cultural diversity as well as hunt behavior. Besides, there are four hunt activities (i.e., chasing, driving, attacking, and blocking) to characterize the behavior of chimps and their prey.

B. RESEARCH GAP AND MOTIVATION

Table 1 introduces a comparison between the motivation of this study and other previous studies. The research gaps of previous studies can be summarized as follow:-

- Most previous studies depended on conventional controllers (e.g., PID and MPC controllers). However, few studies applied the optimal MPC controller.

- Previous studies related to using optimal MPC controllers depended on traditional and heuristic optimization techniques that require selecting parameters in optimization algorithm software. So, this study applies a meta-heuristic optimization algorithm with additional features, such as a short time to achieve the best solution and a high explosion and convergence rate.
- Few previous studies have considered the effect of system uncertainties and nonlinearities.
- Few LFC studies have validated the effectiveness of the considered controller in multi-area interconnected power systems.

Furthermore, the power system grid has become more complex as the load and generation sources have expanded. As a result, to deal with the system complexity, system parameter variations, and high fluctuations caused by renewable penetrations, traditional control techniques should be replaced by effective ones in modern power systems. Motivated by these observations, this article introduces a new robust controller that combines MPC with the LQG control technique for frequency regulation of modern power grids considering nonlinearities and loads/RESs uncertainties. Additionally, applying a novel algorithm called the chimp optimization algorithm (ChOA) for fine-tuning the constraints of the proposed robust controller (i.e., MPC-LQG) considering wind power interpenetrating, system uncertainty, as well as nonlinearity impacts.

C. CONTRIBUTION AND PAPER ORGANIZATION

According to the above analysis, this study can contribute to the subsequent points:

i. Propose a new optimal robust controller that combines MPC with the LQG controller for enhancing the frequency regulation of power grids while accounting for high wind power penetration.
ii. The proposed controller (i.e., MPC-LQG) is optimally determined based on a novel algorithm, referred to as ChOA algorithm, to reduce the integral time-weighted absolute error (ITAE) objective function of the system frequency. Where the ChOA algorithm has been used to achieve the desired target. It is the first time to apply this algorithm to select optimal parameters for LFC problems.
iii. System nonlinearities (i.e. GRC and GDB) and system uncertainties (i.e. system parameters variations) are considered while designing the proposed controller.
iv. The effectiveness of the proposed robust MPC-LQG controller is tested and verified through multi-area interconnected power systems (e.g., single-area and two-area power systems).
v. Comparing with other controllers that were used in LFC studies for improving the system performance (e.g. conventional integral controller and MPC controller).

This article is prearranged as follows: the structure and modeling of the studied power grid are characterized in section 2. Furthermore, the methodology of the proposed control system and the chimp optimization algorithm are clarified in section 3. Moreover, the simulation results considering different operating conditions are addressed in section 4. Section 5 concludes the overall conclusion.

II. POWER SYSTEM DYNAMICS

A. MODELLING OF THE STUDIED SYSTEM

This study introduces a hybrid power grid that includes a thermal power plant and wind farms as a test system. The rated power capacity of the single-area power system is 2000 MVA. Furthermore, Fig. 1 shows the model of the considered power grid. Additionally, the block diagram of the considered power grid considering wind energy is displayed in Fig. 2. Also, Table 2 displays the considered system parameters.

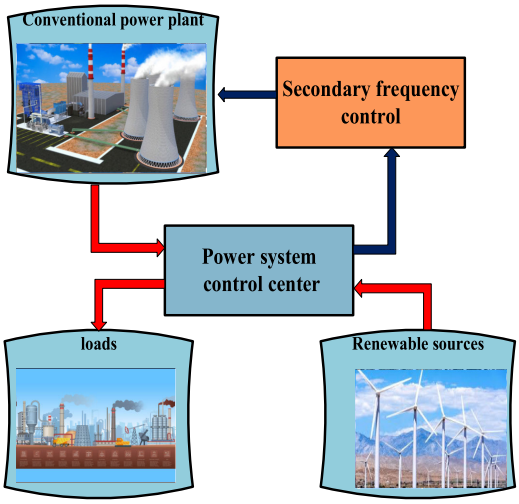

FIGURE 1. The model of the considered power grid.

The studied power system's mathematical equations can then be described accordingly:

The governor model of the thermal plant can be defined as follows:

$$\Delta \dot{P}_g = \left(\frac{1}{T_g}\right).\Delta P_C - \left(\frac{1}{R.T_g}\right).\Delta F - \left(\frac{1}{T_g}\right).\Delta P_g \quad (1)$$

The turbine model of the thermal plant can be defined as follows:

$$\Delta \dot{\mathrm{P}}_{\mathrm{m}} = \left(\frac{1}{\mathrm{T_t}}\right).\Delta \mathrm{P_g} - \left(\frac{1}{\mathrm{T_t}}\right).\Delta \mathrm{P_m} \quad (2)$$

The frequency fluctuations can be defined as follows:

$$\Delta \dot{\mathrm{F}} = \left(\frac{-\mathrm{D}}{2\mathrm{H}}\right).\Delta \mathrm{F} + \left(\frac{1}{2\mathrm{H}}\right).\Delta \mathrm{P_m} + \left(\frac{1}{2\mathrm{H}}\right).\Delta \mathrm{P_{WT,1}} + \left(\frac{1}{2\mathrm{H}}\right).\Delta \mathrm{P_{WT,2}} - \left(\frac{1}{2\mathrm{H}}\right).\Delta \mathrm{P_L} \quad (3)$$

Here, H represents the equivalent inertia constant, D represents the damping coefficient, and R represents the speed regulation. Moreover, the state space of the system under study could be expressed according to previous equations

and Fig. 2 as follow [23]:

$$\dot{X} = AX + BU + EW \tag{4}$$

$$Y = CX + DU \tag{5}$$

Here, X represents the state vector, Y denotes the control output vector, U represents the control input signal, W represents the disturbance vector, B indicates the control output vector, E relates to the disturbance input, C relates to the output measurement.

$$\begin{bmatrix} \Delta\dot{F} \\ \Delta\dot{P}_m \\ \Delta\dot{P}_G \end{bmatrix} = \begin{bmatrix} \frac{-D}{2H} & \frac{1}{2H} & 0 \\ 0 & \frac{-1}{T_t} & \frac{1}{T_t} \\ \frac{-1}{R.T_g} & 0 & \frac{-1}{T_g} \end{bmatrix} \times \begin{bmatrix} \Delta F \\ \Delta P_m \\ \Delta P_G \end{bmatrix} + \begin{bmatrix} 0 & \frac{-1}{2H} \\ 0 & 0 \\ \frac{1}{T_g} & 0 \end{bmatrix} \times \begin{bmatrix} \Delta P_C \\ \Delta P_L \end{bmatrix} \tag{6}$$

$$Y = [1 \quad 0 \quad 0] \times X \tag{7}$$

B. WIND TURBINE MODEL

The oscillations of the wind power can be derived from the simplification model shown in Fig. 3. Here, the white noise block is used to produce random speed. In addition, the random output speed is multiplied by the real wind speed. Then, the resulting signal is the input of the wind turbine generator to estimate the random wind output oscillations [23].

The output power of the wind turbine (P_W) can be expressed as following [10]:

$$P_W = \frac{1}{2}\rho A_T V_W^3 C_P(\lambda, \beta) \tag{8}$$

Here, $C_P(\lambda, \beta)$ represents the rotor blades power coefficient, and can be defined as following [10], [23]:

$$C_P(\lambda, \beta) = C_1 \times \left(\frac{C_2}{\lambda_I} - C_3\beta - C_4\beta^2 - C_5\right) \times e^{\frac{-C_6}{\lambda_I}} + C_7\lambda_T \tag{9}$$

where ρ is the air density in (kg/m3), A_T is rotor swept area (m2), V_W is rated wind speed in (m/s), $C_1 - C_7$ are the turbine coefficients, β symbolizes pitch angle, λ_T appertains optimally to the tip-speed ratio (TSR) and could be expressed

TABLE 1. Comparison between this study and other previous studies.

Properties	[30]	[31]	[32], [33]	[34]	[35]	[42]	[39]	This study
Controller type	Conventional MPC controller			An adaptive MPC controller		Optimal MPC controller		Optimal MPC-LQG controller
Controller design depend on	Designer experience			Genetic algorithm	A recursive algorithm	Sooty terns optimization algorithm	Bat inspired algorithm	ChoA algorithm
Renewable energy penetration	Not considered	High penetration	Low penetration				Not considered	High penetration
Effect of system uncertainties	Considered	Not considered	Considered	Not considered	Considered	Not considered		Considered

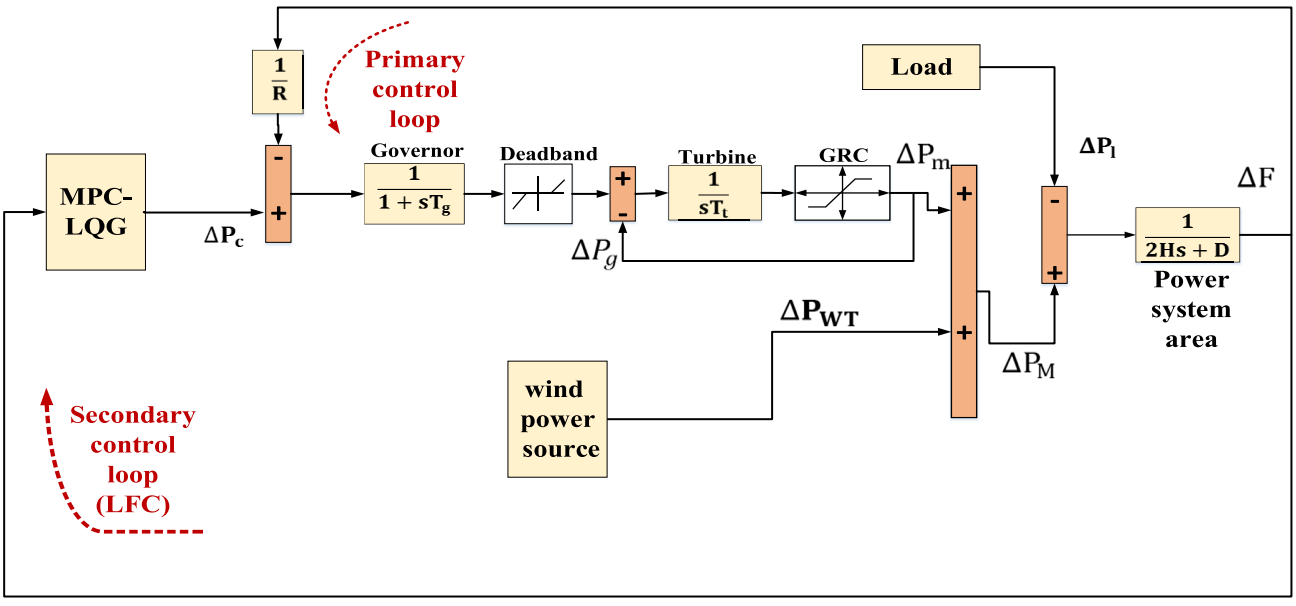

FIGURE 2. The block diagram of the considered single area power grid.

TABLE 2. Parameters for the single-area power system under analysis.

Parameters	Value
D (pu.MW/Hz)	0.015
H (pu. MWs)	0.08335
T_g (sec)	0.08
T_t (sec)	0.4
R (Hz/ pu.MW)	3
GRC (pu.MW per minute)	10%
GDB (Hz)	0.006

as follow:

$$\lambda_T = \lambda_T^{OP} = \frac{\omega_T \times r_T}{V_W} \tag{10}$$

Here, r_T represents the rotor radius, and λ_I is an intermittent TSR. It can be expressed as shown in equation (11):

$$\frac{1}{\lambda_I} = \frac{1}{\lambda_T + 0.08\beta} - \frac{0.035}{\beta^3 + 1} \tag{11}$$

In addition, the parameters of the wind turbine are displayed in Table 3. Moreover, the output of the wind turbines is 6 MW, which is 8 wind turbines of 0.75 MW per wind turbine.

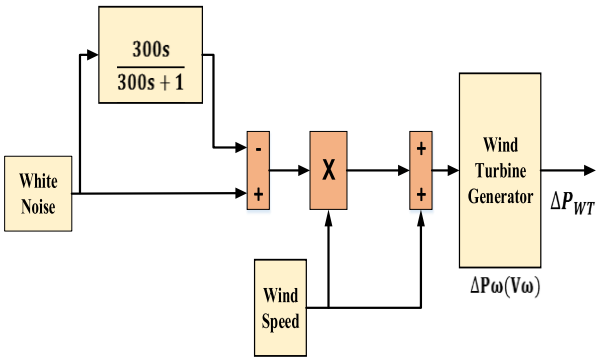

FIGURE 3. The estimated model of the wind power source.

TABLE 3. The nominal parameters of the wind turbine [23].

Parameter	Value	Parameter	Value
P_w	750 KW	c_2	116
V_w	15m/s	c_3	0.4
ρ	1.225 kg.m^3	c_4	0
A_T	1648m^2	c_5	5
r_T	22.9 m	c_6	21
n_T	22.5 rpm	c_7	0.1405
c_1	-0.6175		

III. PROPOSED MPC-LQG CONTROLLER DESIGN

A. PROPOSED CONTROL STRUCTURE

In this article, the MPC-LQG controller is proposed for boosting the system stability taking into account system nonlinearities, uncertainties, and high RESs penetration. Where the proposed controller combines MPC and the LQG controllers to gain the merits of the multiple controllers. Moreover, Figure 4 displays the simplified block diagram of the proposed MPC-LQG controller. It is clear that the proposed controller depends on the control horizon (M), prediction horizon (P), sampling time (t_s), weighting factors for the MPCQ_{MPC}, R_{MPC}, and matrices of the control and the weighting for the LQG controller Q_{LQG}, R_{LQG}. Furthermore, the concept of the proposed controller design is illustrated in the flowchart in Figure 5.

The proposed controller blends the merits of both the MPC and LQG approach. The MPC has many merits such as rapid response, simplicity, ease of structure, and good handling of the system nonlinearities and constraints. While the LQG controller has been used to link with the MPC due to substantial advantages such as:

i. Supplying a time-varying input signal in every instant allows the coordination to track the correct path.
ii. Ability to minimize the cost functions during transient periods.
iii. Reliability and ability to select various controller configurations of the controller concerning the non-uniqueness properties of optimal control.

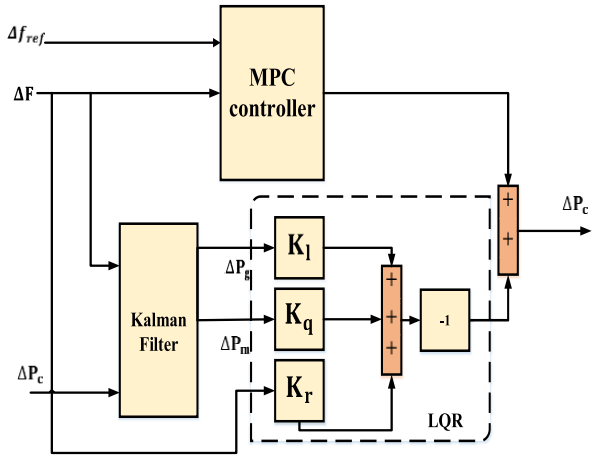

FIGURE 4. The proposed MPC-LQG controller's simplified block diagram.

The design process of the proposed MPC-LQG controller has been conducted in MATLAB software using the MPC toolbox and the LQR function. In addition, the calculations of the design process can be summarized in Figure 5. In this regard, the MPC strategy consists of the predictive and control units. The predictive unit comprises system and disruption models that predict future system behavior based on overall performance, calculated disturbance, undetermined disturbance, and control signal over the finite forecast horizon. The control unit uses the expected output as known parameters in an optimization problem that minimizes the objective function in the existence of system constraints. The solution to his problem leads to an optimal control sequence over the control horizon.

The first element of this series is inserted into the system and the whole process is repeated at the next sampling interval when the forecast horizon carries one sampling interval forward [46], [47]. The MPC model also excludes the

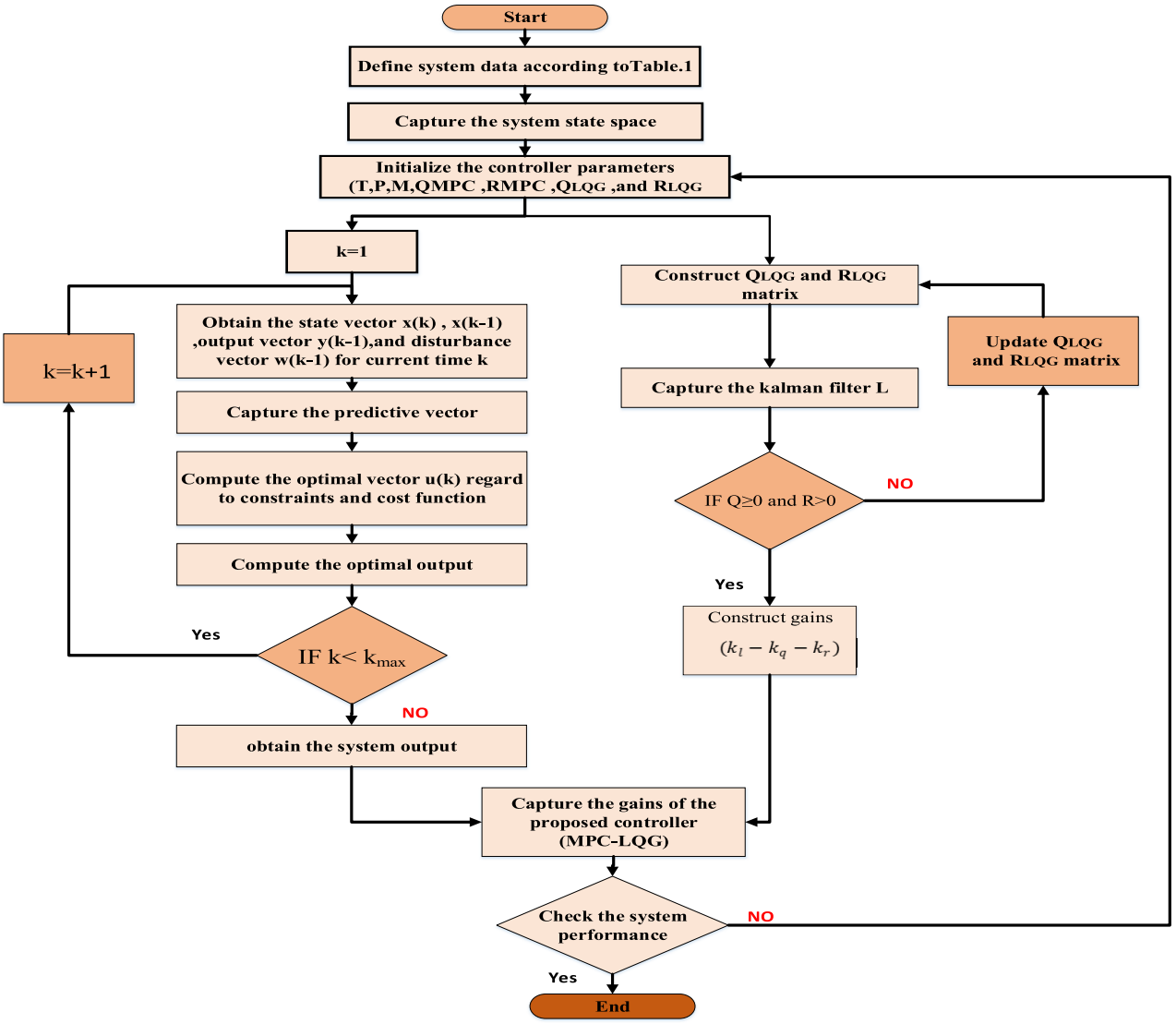

FIGURE 5. The procedure of designing the proposed MPC-LQG controller.

(plant model – input disturbance model – output disturbance model – measurement disturbance model) as shown in detail in Figure 6.

In general, the design of the MPC controller is based on a time-invariant plant system model and can be described as follows:

$$x_p(k+1) = A_p x_p(k) + B_{pu} u(k) + B_{pv} v(K) + B_{pd} d(k) \quad (12)$$

$$y_p(k) = C_p x_p(k) + D_{pu} v(k) + D_{pv} u(k)\, D_{pd} d(k) \quad (13)$$

$$C_p = S_0^{-1} . C \quad (14)$$

where S_0 represents a diagonal matrix of output scale factors, x_p represents the system state vector, and u (k) , d (k) v (k) are; the vector with manipulated control output, the vector with unmeasured disturbance, and the vector with measured disturbances, respectively. Here, B_{pu}, B_{pv}, and B_{pd} are corresponding columns of B. Also, D_{pu}, D_{pv}, and D_{pd} are the corresponding columns of D. Moreover, the MPC transforms the disturbance model into a linear state-space structure, which has the same procedures for transforming the model system and is:

$$x_d(k+1) = A_d x_d(k) + B_d w_d(k) \quad (15)$$

$$d(k) = C_d x_d(k) + D_d w_d(k) \quad (16)$$

Here, d (k) represents the unmeasured disturbance, w_d (k) represents the dimensionless noise inputs, x_d (k) represents the input disturbance model states, and A_d, B_d, C_d, D_d are constant state-space matrices.

Then, the MPC transforms the noise model into a linear time-invariant state-space system, and the outcome is

$$x_n(k+1) = A_n x_n(k) + B_n w_n(k) \quad (17)$$

$$y_n(k) = C_n x_n(k) + D_n w_n(k) \quad (18)$$

where, A_n, B_n, C_n, D_n are constant state-space matrices, $x_n(k)$ represents the vector of the noise model state, $y_n(k)$ represents a vector of noise signals to be added to the measured plant outputs, and $w_n(k)$ is a vector dimensionless of the noise input.

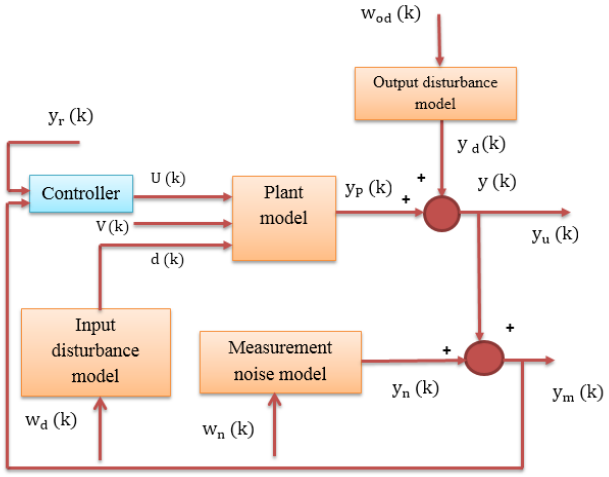

FIGURE 6. The block diagram of MPC in the state-space model.

By applying the LQG controller to achieve the desired goal through reducing J the quadratic cost function, this was accomplished by achieving the optimal solution of the cost function as follow:

$$J = \int_{t_o}^{t_f} (\acute{x}Q_{LQG}x + uR_{\acute{L}QG}u + 2X\grave{N}u)dt \tag{19}$$

Here, Q_{LQG} and R_{LQG} are the weigh and the control matrices respectively. Then, to reduce the value of J, it is necessary to select the optimum value of the K control input.

$$u(t) = -K(t)\,x(t) \tag{20}$$

Optimal state feedback u (t) could not be completed without a proper state measurement. In our analysis, the variables are chosen to be Δf, ΔP_m, and ΔP_g. In addition, Δf and ΔP_c are known to be input signals that are fed to the Kalman estimator.

$$\hat{x} = \begin{bmatrix} \Delta\hat{f} & \Delta\hat{p}_m & \Delta\hat{p}_g \end{bmatrix} \tag{21}$$

Then, the estimate of the state in equation (21) can be derived as follow:

$$\left(\dot{\hat{x}}\right) = (A - Bk - LC)\,\hat{x} + Ly \tag{22}$$

Briefly, the proposed MPC-LQG controller completed using two commands in MATLAB "$[K]$ = LQR (A, B, Q_{LQG}, R_{LQG})", and "MPCobj = mpc (plant, t_s, P, M, W)" where the Q_{LQG}, R_{LQG}, t_s, P, M, and W can be selected by applying different optimization algorithms.

In this analysis, the novel optimization algorithm; referred to as ChOA, is used to select the optimal parameters of the proposed controller. In addition, the ITAE function is considered as an objective function of the optimization problem to help in selecting the optimal parameters of the proposed MPC-LQG controller due to its good properties (i.e. faster time, and producing smaller overshoot and oscillations compared to other objective functions forms) in order to achieve better rendering [48]. Moreover, the ITAE can be expressed as follows:

$$ITAE = \int_0^{tsim} t.(|\Delta f|).dt \tag{23}$$

where, Δf, t_{sim} are frequency deviation of the system and the simulation time, respectively. The constraints of the proposed MPC-LQG controller are defined in (24).

$$\begin{cases} t_s^{min} \le t_s \le t_s^{max} \\ P^{min} \le P \le P^{max} \\ M^{min} \le M \le M^{max} \\ Q_{MPC}^{min} \le Q_{MPC} \le Q_{MPC}^{max} \\ R_{MPC}^{min} \le R_{MPC} \le R_{MPC}^{max} \\ Q_{LQG}^{min} \le Q_{LQG} \le Q_{LQG}^{max} \\ Q_{LQG}^{min} \le Q_{LQG} \le Q_{LQG}^{max} \end{cases} \tag{24}$$

B. THE PROPOSED CHOA ALGORITHM

1) DESCRIPTION OF CHOA ALGORITHM

The ChOA was influenced by how chimpanzees live in nature. Chimpanzees are similar to human living relatives. The key feature of the chimp's colony fusion is defined by four types: the driver, the barrier, the chaser, and the attackers. They each have unique capacities, but for good hunting, these differences are important. Where the chimp's drivers pursue their beast while trying to grape up. Chimp's barriers are mounted in a forest to construct a bridge through the succession of the predator. Then, chasers run quickly to grab up their predator. Lastly, the chimp's attackers predict their breakup path from the prey to the chasers or the lower canopy. Chimpanzee hunting is typically divided into two principal stages: exploration and exploitation of the prey. Where, the exploration stage combines driving, blocking, and cashing. Besides, the stage of exploitation consists of prey attack [45].

C. ALGORITHMCHOA MATHEMATICAL MODELLING

1) THE PREY DRIVING AND CHASING

During the stages of discovery and processing, the predator is hunted. Moreover, the mathematical modeling of driving as well as chasing the predator is set out in the equations below.

$$d = |c.X\_prey(t) - m.X\_chimp(t_i)| \tag{25}$$

$$X_{chimp}(t_i + 1) = X_{prey}(t_i) - a.d \tag{26}$$

Here, t_i denotes iteration of the current number, X_{prey} symbolizes the position vector of the predator, X_{chimp} indicates the vector of chimp position, and (a, d, *and* m) is the coefficient vectors and deliberated according to the next relations.

$$a = 2.f.r_1 - f \tag{27}$$

$$c = 2.r_2 \tag{28}$$

$$m = chaotic\_value \tag{29}$$

Depending on the iteration process, f decreased from 2.5 to 0. As well, r_1 as well as r_2 represent the unsystematic vectors and they have values ranging from 0 to 1.

Decisively, m represents a chaotic vector identified by different chaotic maps, reflecting the impact of sexual motivation in the hunting stage of chimpanzees. In addition, two distinct versions of the ChOA with different independent groups are chosen to provide better results in optimization problems. In addition, these versions are shown in Table 4 [45].

TABLE 4. The two versions of the ChOA [45].

Groups	ChoA-1	ChoA-2
Group1	$1.95 - 2t_i^{\frac{1}{4}}/T^{1/3}$	$2.5 - (2\log(t_i)/\log(T))$
Group 2	$1.95 - 2t_i^{\frac{1}{3}}/T^{1/4}$	$\left(-\frac{2t_i{}^3}{T^3}\right) + 2.5$
Group 3	$\left(-\frac{3t_i{}^3}{T^3}\right) + 1.5$	$0.5 + 2\exp\left[-(\frac{4t_i}{T})^2\right]$
Group 4	$\left(-\frac{3t_i{}^3}{T^3}\right) + 1.5$	$2.5 + 2(\frac{t_i}{T})^2 - 2(\frac{2t_i}{T})$

Here, T symbolizes the cumulative number of iterations that can be performed, as well as t_i designates the number of recent iterations. The chimpanzees shift their locations to the locus of the predator. It should be noted that chimpanzees may access the random vectors r_1 and r_2 at any location between the points. Consequently, chimpanzees can therefore alter their position in the prey area based on previous equations.

2) CHASINGTHE FORM OF THE ATTACKING METHOD

The chimpanzees can explore and surround the position of the prey (by walking, blocking, and hunting). Attacking chimps are responsible for hunting. Chimps are rarely involved in the hunting process as drivers, barriers, or hunters. Regrettably, there is no information on the optimal position in the prey area. Furthermore, it is presumed that the first attacker (the best outcome accessible), the pilot, the fence, and the hunter are more aware of the position of potential prey, according to equations 30 to 32. While, the ending point is chosen at a random within a circle marked by the attacker, the barrier, the chaser, and the driver's chimp locations. In brief, the four strongest classes determine the location of the prey, and the other chimps refresh their locations in their vicinity at random.

$$\begin{aligned} d_{Attacker} &= |c_1.X_{Attacker} - m_1.X|, \\ d_{Barrier} &= |c_2.X_{Barrier} - m_2.X| \end{aligned} \tag{30}$$

$$\begin{aligned} d_{Chaser} &= |c_3.X_{Chaser} - m_3.X|, \\ d_{Drier} &= |c_4.X_{Drier} - m_4.X| \end{aligned} \tag{31}$$

$$\begin{aligned} X_1 &= X_{Attacker} - a_1(d_{Attacker}), \\ X_2 &= X_{Barrier} - a_1(d_{Barrier}) \\ X_3 &= X_{Chaser} - a_1(d_{Chaser}), \end{aligned} \tag{32}$$

$$X_4 = X_{Drier} - a_1(d_{Drier}) \tag{33}$$

$$X(t+1) = \frac{X_1 + X_2 + X_3 + X_4}{4} \tag{34}$$

3) THE FORM OF THE PREY ATTACKING

At the last moment, when the prey ends shifting, the chimpanzees attack the prey and end their search. Where the process of updating location is called the utilization process. The ChOA helps the chimpanzee to upgrade their locations to attack, barrier, chaser, and driver chimpanzee positions and attack the prey according to their location.

4) SOCIAL INCENTIVE

At the final stage, the chimpanzees are relieved of their hunting obligations. They attempt to get meat chaotically when they are satisfied and eventually socially motivated. Moreover, more than chaotic maps are used for boosting the efficiency of ChOA. Through the optimization process, 50% of the time is used to select the chimp position between the normal upgrading location and the chaotic layout, which can be represented using the below formula:

$$X_{chimp}(t_i + 1) = \begin{cases} X_{prey}(t_i) - a.d & \text{if } \mu < 0.5 \\ \text{chaotic\_alue} & \text{if } \mu > 0.5 \end{cases} \tag{35}$$

Here, μ is a random number that relies on between 0 and 1. In short, the ChOA discovery process starts with the generation of a probabilistic community of chimpanzees (candidate outcomes).

The chimpanzees are then indiscriminately separated into four predetermined individual classes called attacker, barrier, chaser, and driver. Each chimpanzee's f value is apprised through using community. For the duration of the iteration, attacker, barrier, hunter, and driver chimpanzees guesstimate the probable position of the prey. Every chimpanzee can narrow its gap with the prey. Adaptive tuning of the c and m vectors induces local implementations and a quick convergence curve at the same time. For improving the exploitation phase and attack the prey, the f value has been reduced from 2.5 to 0.

D. IMPLEMENTATION OF THE PROPOSED CONTROLLER-BASED CHOA ALGORITHM

The steps of designing the proposed controller-based ChOA algorithm are described in the flow chart in Figure 7. The ChOA-1 is the algorithm that has been applied in this study. Furthermore, Figure 8 shows the process of selecting the parameters of the proposed controller-based ITAE objective function. Moreover, the maximum and minimum values of the controller parameters are listed in Table 5.

IV. STABILITY AND ROBUSTNESS OF THE PROPOSED CONTROL STRATEGY

One of the key considerations of a closed-loop system is stability. In several methods were described in detail for analysing the stability of linear and nonlinear systems [49]. The Lyapunov method is the most commonly used method in

analysis. This method relies on gazing for a positive definite function of the state with a negative time derivative. For any linear system, the time-invariant state space is expressed as

$$\dot{x}(t) = Ax(t) + Bu(t) \tag{36}$$
$$Y(t) = Cx(t) + Du(t) \tag{37}$$

For the Lyapunov function

$$V(x) = x^T Px \tag{38}$$

wherever, P indicates to the symmetric positive definite matrix and the time derivative of $V(x)$ will be negative for $\forall x \neq 0$.

$$\frac{dV(x)}{dt} = \dot{x}^T Px + x^T P\dot{x}$$
$$= x^T \left(A^P P + PA\right) x < 0, \quad \forall x \neq 0 \tag{39}$$
$$A^T P + PA < 0 \tag{40}$$

Furthermore, the symmetric positive matrix P is expressed as:

$$P = \sum_{j=1}^{n} \sum_{i \geq j}^{n} P_{ij} E^{ij} \tag{41}$$

Here, E_{ij} can be defined as a matrix with unique items and zero other items, as well as P_{ij} is the (i, j) for the items of P. Thus, E^{ij} forms a substratum for (n × n) matrices. At that moment, replacing of P in its origin matrix:

$$A^T P + PA$$
$$= A^T \left(\sum_{j=1}^{n} \sum_{i \geq j}^{n} P_{ij} E^{ij}\right) + A \left(\sum_{j=1}^{n} \sum_{i \geq j}^{n} P_{ij} E^{ij}\right)$$
$$= \sum_{j=1}^{n} \sum_{i \geq j}^{n} P_{ij} (A^T E^{ij} + AE^{ij}) < 0 \tag{42}$$

Then, $F(x)$ can be expressed as follows:

$$F(x) = F_0 + \sum_{i=1}^{m} x_i F_i > 0 \tag{43}$$

wherever, $F_0 = 0$ as well as $F_k = -A^T E^{ij} - E^{ij} A$ for k = 1 . . . m.

Conferring to (43), the origins of vector (x) are P_{ij}, $i \geq j$ stacked up each other.

Furthermore, the state space formula for the consideration system can be expressed according to (34) as follows:

$$\dot{\boldsymbol{x}} = \begin{bmatrix} -12.5 & 0 & 0 \\ 12.5 & -3.333 & 0 \\ 0 & 3.333 & -0.0899 \end{bmatrix} \boldsymbol{x} + \begin{bmatrix} 0 & 0 & 1 \end{bmatrix}^{\boldsymbol{T}} \boldsymbol{u} \tag{44}$$

Consistent with (20), the feedback gain is specified via the next equations:

$$k = -R^{-1} B^T P = -R^{-1} \begin{bmatrix} 0 & 0 & 1 \end{bmatrix} \begin{bmatrix} P_{11} & P_{12} & P_{13} \\ P_{21} & P_{22} & P_{23} \\ P_{31} & P_{32} & P_{33} \end{bmatrix}$$
$$k = -R^{-1} a \begin{bmatrix} P_{13} & P_{23} & P_{33} \end{bmatrix} = -\begin{bmatrix} k_l & k_q & k_r \end{bmatrix}$$
$$k_{lqr} = \begin{bmatrix} 0.2990 & 0.6621 & 0.1488 \end{bmatrix} \tag{45}$$

However, the closed loop system stability can be verified by the Lyapunov criterion. P is defined by the LMI in (43) as:

$$P = \begin{bmatrix} 0.0123 & 0.012 & 0.014 \\ 0.011 & 0.02 & 0.105 \\ 0.001 & 0.002 & 0.011 \end{bmatrix} \tag{46}$$

The configuration in (44) is practically stable according to the Lyapunov criterion, as seen in (46), where all eigenvalues are positive.

Furthermore, the Bode plot of the considered system loop gains with and without the proposed MPC-LQG controller has been shown in Figure 9.

V. SIMULATION STUDY AND REVIEW OF SYSTEM PERFORMANCE

The MATLAB program is used as an assistant tool to conduct the simulation study and evaluate the performance of the considered systems under study. While the model of the studied system is established using MATLAB/SIMULINK, and the ChOA code is written using MATLAB/ M.FILE. Additionally, the ChOA code is gassed with the model to complete the optimization procedure considering system uncertainties and nonlinearities, the wind power penetration, and different load disturbances (i.e. series load – random load). The MATLAB program has been implemented on a Laptop with core i5, and 6 GB ram. Furthermore, the performance of the proposed MPC-LQG controller-based ChOA was compared to the performance of other control techniques (i.e. Integral controller, conventional MPC). In addition, the dynamic coefficients of ChOA-1 that were used in this study are shown in Figure10. Furthermore, the studied power grid is subjected to several operating scenarios.

A. SCENARIO 1. PERFORMANCE EVALUATION OF THE SYSTEM UNDER CONSIDERATION USING VARIOUS OPTIMIZATION TECHNIQUES

This scenario demonstrates the effectiveness of the proposed ChOA algorithm relative to other optimization algorithms. Furthermore, The effectiveness of the proposed ChOA technique is checked by contrasting the performance of the considered power grid with the proposed MPC-LQG controller-based ChOA algorithm with other optimization algorithms (i.e. particle swarm optimization (PSO), gray wolf optimization (GWO), and ant lion optimizer (ALO)). Wherever the performance of the system under consideration is evaluated taking into consideration system nonlinearities (e.g. GRC and GDB), and a 2% of step load perturbation at t = 3 sec. The convergence curves of the proposed ChoA algorithm and other optimization algorithms are displayed in Figure 11. Also, Table 6 shows the optimum parameters of the proposed MPC-LQG controller considering different optimization techniques. As well, the considered system performance based on the ChOA algorithm and other optimization techniques is displayed in Figure 12. It is obvious from the previous results, that the proposed ChoA

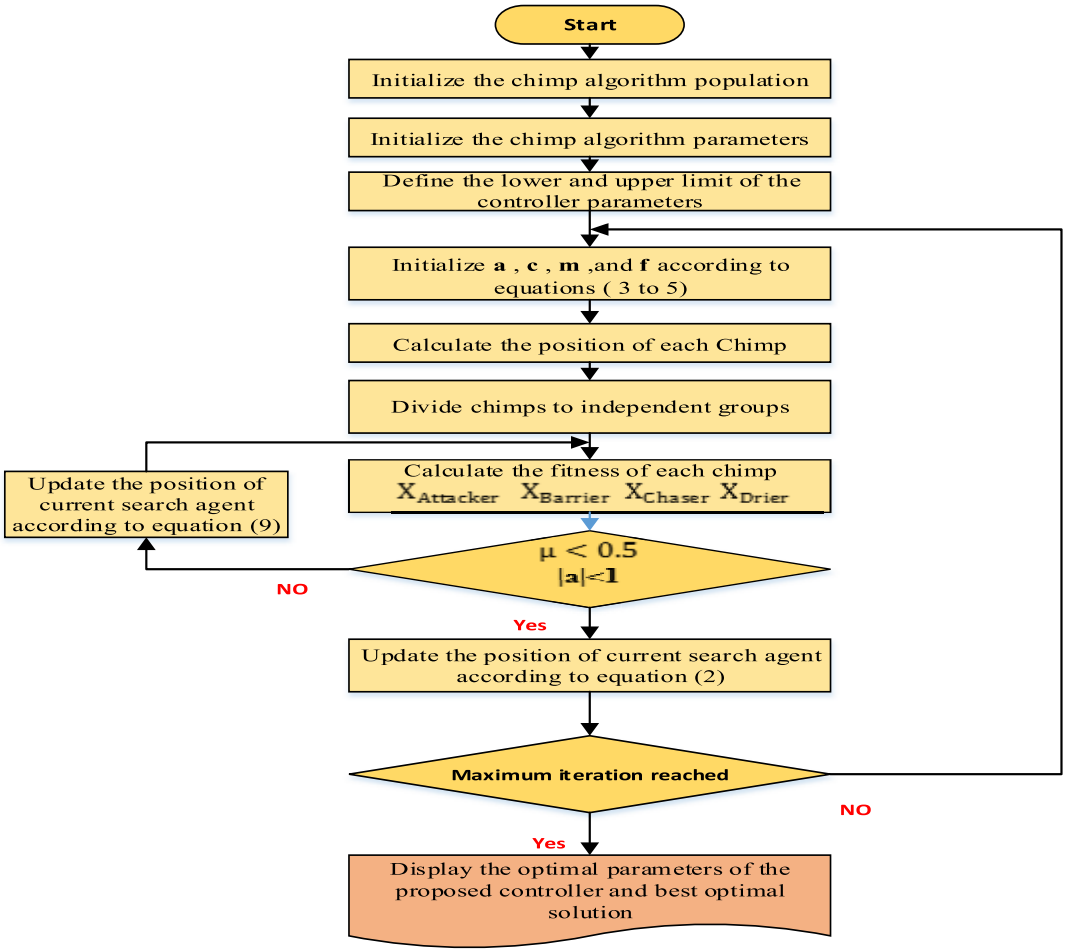

FIGURE 7. Procedures of designing the proposed controller based on the ChOA algorithm.

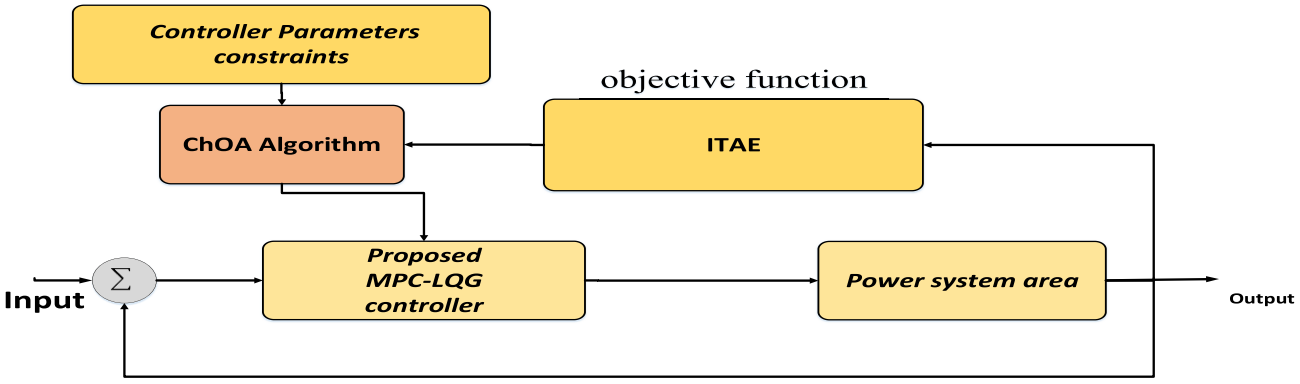

FIGURE 8. The process of determining the optimal constraints of the proposed MPC-LQG control.

algorithm is faster and achieves a better objective function value than other optimization algorithms. Figure 11 clears that the system performance relied on the suggested algorithm provides the lower value of frequency deviations in comparison with other studied controllers. The frequency deviations with the proposed controller-based PSO, proposed controllers-based GWO, proposed controller-based ALO are ±0.063 Hz, ±0.053 Hz, ±0.035 Hz respectively. While the frequency deviations with the proposed controller-based proposed ChOA algorithm is ±033Hz. The MPC-LQG controller-relied on ChOA algorithm boosts frequency stability and eliminates the deviations in less time after the subjected disturbance than the other studied controllers. So, the proposed MPC-LQG controller has been used to enhance the system under study stability for various operating situations.

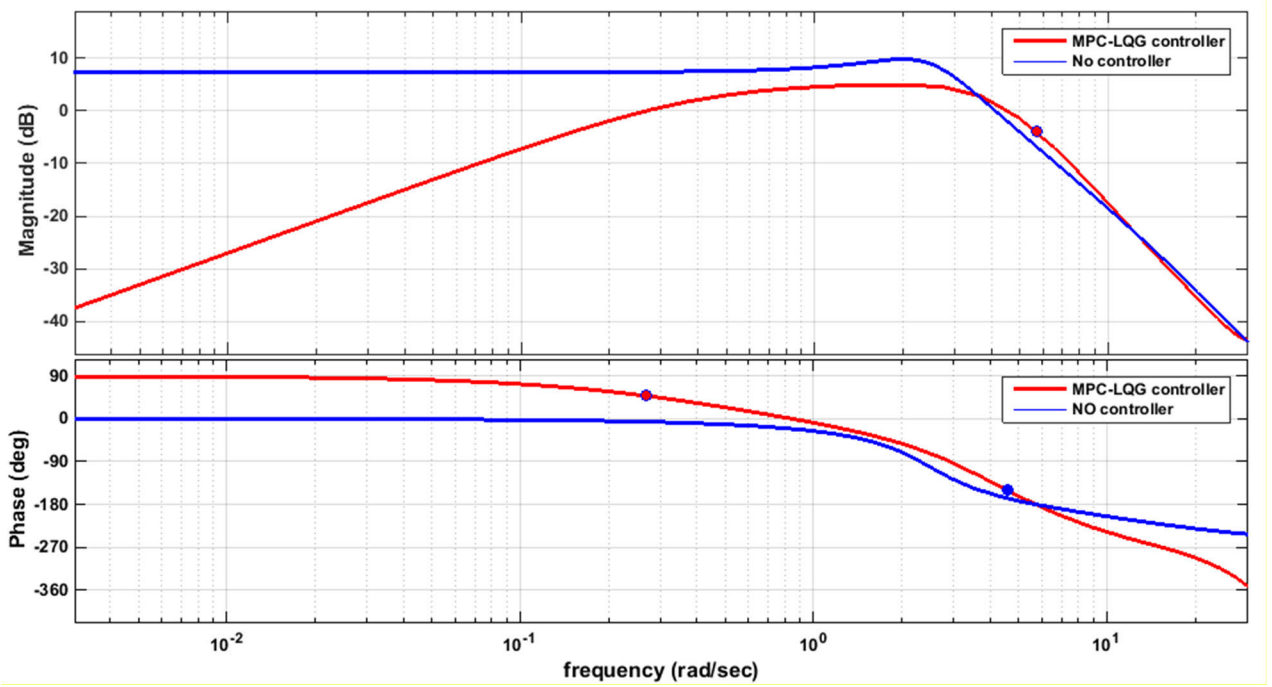

FIGURE 9. The Bode plot of the considered system loop gains with and without the proposed MPC-LQG controller.

TABLE 5. ChOA algorithm and the parameters limit of the proposed controller.

Number of iterations	100
Number of search agents	20
Range of t_s	[0.1 10]
Range of P	[1 20]
Range of M	[1 10]
Range of Q_{MPC}	[1 10]
Range of R_{MPC}	[1 10]
Range of Q_{LQG} matrix	[0 30]
Range of R_{LQG} matrix	[50 300]

B. SCENARIO 2. PERFORMANCE EVALUATION OF THE SYSTEM UNDER CONSIDERATION UNDER DIFFERENT LOAD DISTURBANCES

Many experiments are based on the assumption that the load profile is a step-change disturbance. However, the load disturbance in nature is complex. This scenario introduces three different types of load disturbances (e.g. step load disturbance – series load disturbance – random load disturbance). The system under study based on different control techniques is tested considering different load disturbances. Where the optimal parameter values of the proposed controller, integral controller [46], and conventional MPC [47] are reported in Table 7.

Case A: this case clears the estimation of the system performance-based the proposed controller and other controllers (e.g. integral controller [46], the conventional MPC [47]) under the system's normal parameters, and applying a 2% step load change for the considered system at t = 3 sec. The performance of the studied power grid based on different control techniques, as well as the proposed MPC-LQG controller-based ChOA) for this case is displayed in Figure 13. The previous figure shows that the system performance-based the proposed MPC-LQG controller-based ChOA algorithm is stable in comparison to other studied controllers. Where, the frequency deviations of the system with the integral controller is about ±0.059 Hz, while the system with the conventional MPC controller is about ±0.05 Hz, and the frequency deviations of the system with the proposed controller is about ±0.039 Hz. The proposed controller can effectively for enhancing the frequency of the system.

Case B: the system under study is subjected to a series load disturbance, in this case. The series load disturbances act as a sequence of coercive outages of power units otherwise sudden turn-off demanded loads. Figure 14 shows the studied system performance-based studied control techniques. The simulation results explicate that, the MPC-LQG controller-relied on ChoA technique diminishes the frequency oscillation in less time than other control techniques, the frequency deviations fluctuate in the range ±0.06 Hz. On the other hand, the frequency deviations with an integral controller and conventional MPC controller fluctuate in the range ±0.08 Hz, ±0.07 Hz respectively. Also, the proposed controller eliminates the fluctuations in less time compared to other studied controllers.

TABLE 6. The optimal constraints of the proposed controller-based different optimization techniques.

Optimization algorithm	ITAE	Ts	P	M	R_{MPC}	Q_{MPC}	K_L	K_Q	K_R
ALO	0.2777	1.1917	1.0101	8.8030	1.302	6.3525	0.1624	0.4771	0.2208
PSO	0.3396	3.4428	6.6590	8.5996	4.7445	8.0115	0.0433	0.1404	0.0688
GWO	0.2213	1.1856	10	4.9784	5.2477	7.5393	0.0857	0.2053	0.1572
ChOA (proposed)	**0.1248**	**0.1**	**6.4265**	**4.2116**	**1.0409**	**10**	**0.2844**	**0.4365**	**0.1035**

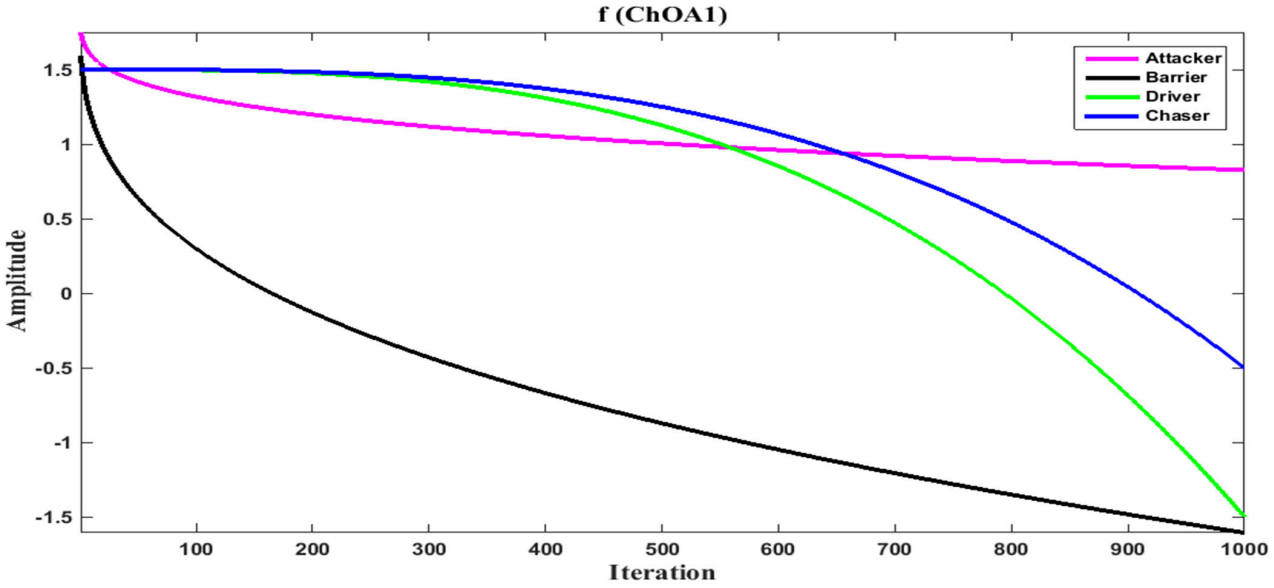

FIGURE 10. The dynamic coefficients of ChOA-1 algorithm.

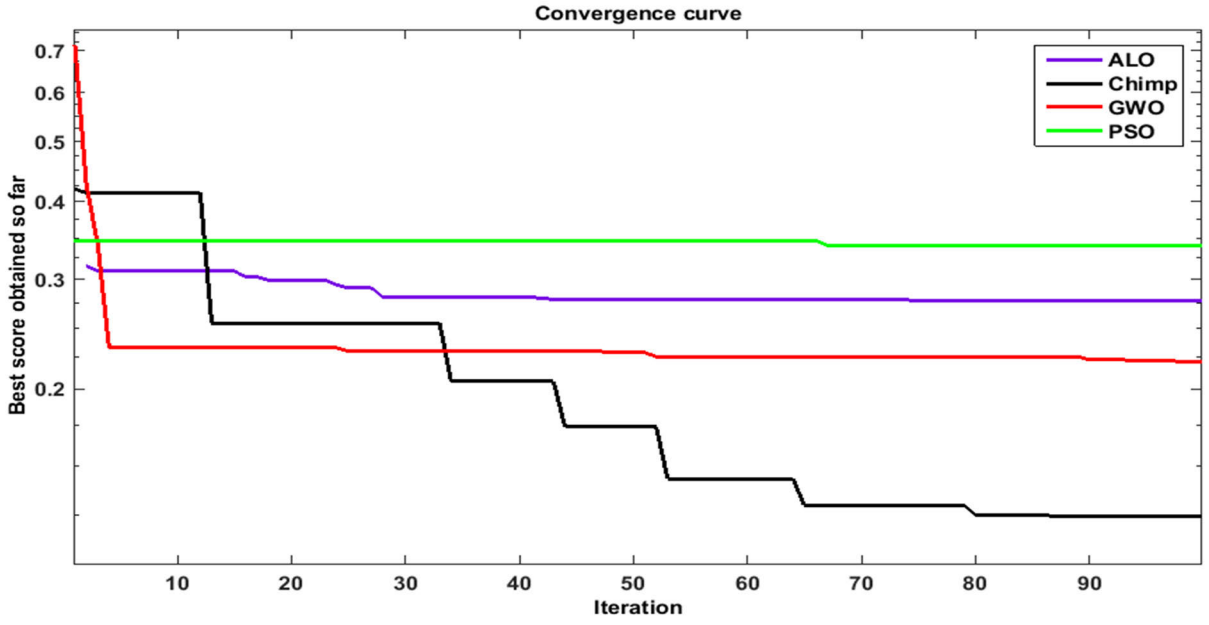

FIGURE 11. The convergence curves of the proposed MPC-LQG controller relied on various optimization techniques.

Case C: the system under study is subjected to a random load disturbance, in this case. while, the random load disturbances is a combination of a ramp load that can characterize the industrial load, as well as a series of step load variations that can characterize a series of coercive outages of power units. Figure 15 displays the applied random load, and the

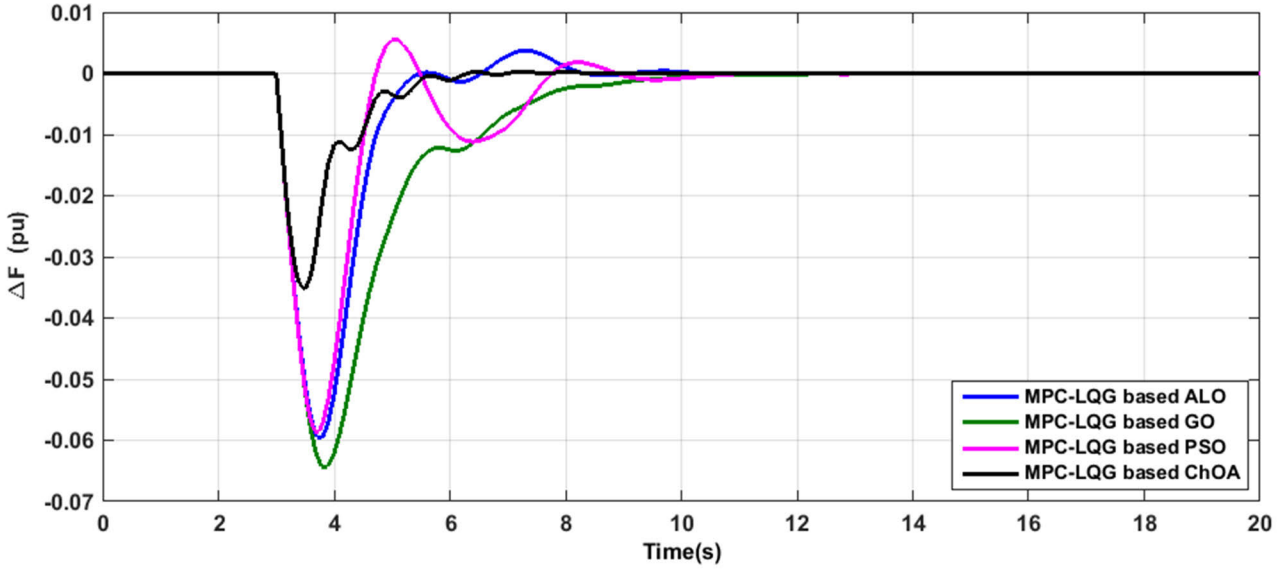

FIGURE 12. The system performance using the proposed MPC-LQG controller-based different optimization techniques.

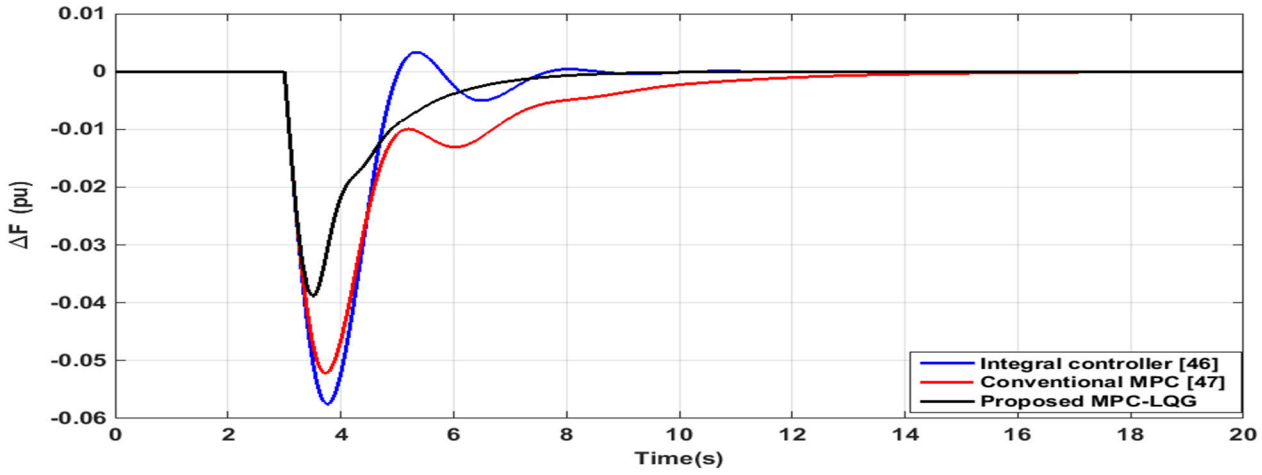

FIGURE 13. Single-area power system performance based on different control techniques for case A, scenario 2.

system performance based on different control techniques for this case. The system frequency fluctuates in range ±0.03 Hz while based the proposed controller, in the range ±0.045 Hz while based the conventional MPC controller, and in the range ±0.057 Hz while based the integral controller. According to these values, the proposed controller is able to deal with load disturbances effectively. Therefore, the system performance based on the proposed controller is faster, and better damped than other studied controllers.

C. SCENARIO 3. PERFORMANCE EVALUATION OF THE SYSTEM UNDER CONSIDERATION UNDER DIFFERENT LOAD VARIATIONS AND SYSTEM UNCERTAINTY

In this scenario, the robustness of the proposed MPC-LQG controller-based ChOA algorithm is estimated under system uncertainty (i.e. system parameters variations). The time constant of both the governor and turbine increase to 150% and 250% from their nominal values, respectively. Also, the damping coefficient of the studied system increases to 0.0195 pu/Mw.Hz. This condition happens while the off-line varying of the turbine as well as the governor parameters. Moreover, the optimal parameter values of the proposed controller and other comparable controllers used in this scenario are listed in Table 7. This scenario is implemented under the following two cases:

Case A: in this case, the proposed controller is tested considering system parameters variations as well as series load disturbances. The simulation results for this case are shown in Figure 16. From figure 16, the performance of the system by the proposed MPC-LQG controller, which is optimally designed based ChOA algorithm is more stable

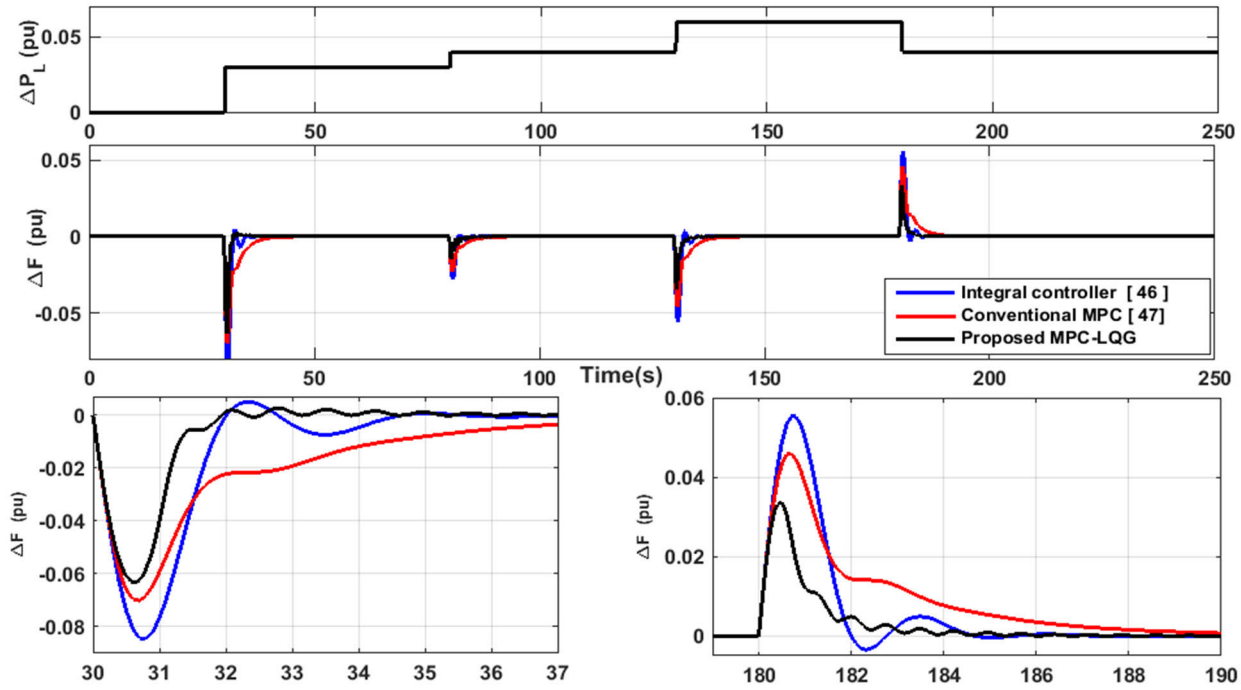

FIGURE 14. The single-area power system performance relied on various control techniques for case B, scenario 2.

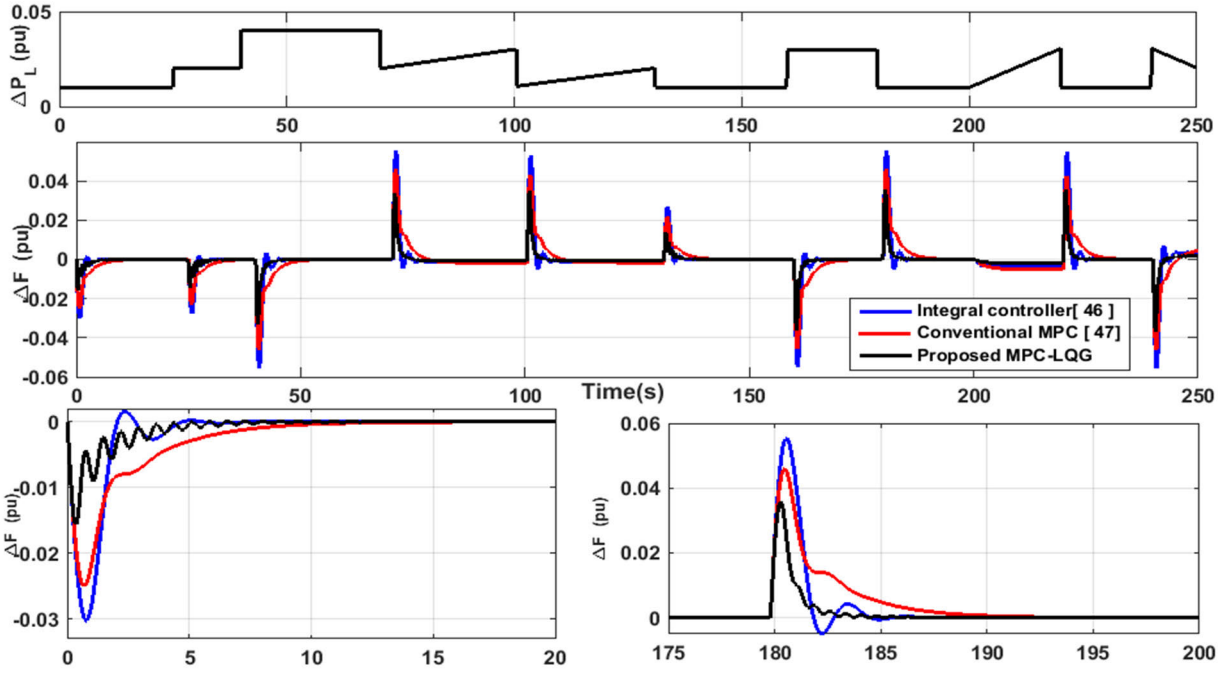

FIGURE 15. The single-area power system performance relied on various control techniques for case C, scenario 2.

and eliminates fluctuations than other studied control techniques. Where, the frequency deviations of the system-based integral controller ±40 Hz, and the frequency deviations of the system-based conventional MPC controller ±0.12 Hz. On the other side the frequency deviations of the system that based on the proposed controller ±0.09 Hz. Besides, the proposed controller diminishes the deviations faster than other control techniques. it is concluded that the best system performance has been achieved by the proposed MPC-LQG controller-based ChOA algorithm.

TABLE 7. The parameters of the proposed controller, integral controller, and conventional MPC controller for single-area power system.

Controller	parameters
The integral controller [46]	$k_i = -0.3$
The conventional MPC [47].	P=10 , M=2 , T_s=0.003 Weights on manipulated variables = 0 , Weights on manipulated variable rates = 0.1 , Weights on the output signals = 1,
The proposed MPC–LQG controller	P=6.465 , M=4.2116 , T_s=0. 1, R_{MPC}= 1.0409 , Q_{MPC}= 10 , K_l= 0.2844 , K_q= 0.4365 , K_r= 0.1035

Case B: in this case, the robustness and effectiveness of the proposed MPC-LQG controller-based ChOA algorithm are validated by applying a random load disturbance to the considered system. The simulation outcomes of this case are displayed in Figure 17. From Figure 17, the conventional MPC controller progresses the frequency response as well as eliminates the frequency deviations in comparison with the integral controller as the frequency deviations based on the conventional MPC controller is about ±0.075 Hz, and the frequency deviations based on the integral controller is about ±25 Hz. it is obvious, the proposed MPC-LQG controller relied on the ChOA algorithm gives superior performance and more elimination in system frequency deviation as the frequency deviation is about ±0.049 Hz.

D. SCENARIO 4. PERFORMANCE EVALUATION OF THE SYSTEM UNDER CONSIDERATION CONSIDERING WIND POWER INTERPENETRATING

The efficacy of the MPC-LQG controller is checked and evaluated considering renewables penetration (i.e. the wind power penetration) as well as different load disturbances. The wind power profile used in this scenario is shown in Figure 18. And then, the resulted wind power fluctuations from two wind farms in this scenario ΔP_w = 0.066 pu. The optimum constraints of the proposed MPC – LQG controller-relied on ChOA under this scenario are listed in Table 8. This scenario is divided into two cases.

Case A: in this case study, the system under consideration is tested by applying a random load variation while considering wind power penetrations. The two wind farms

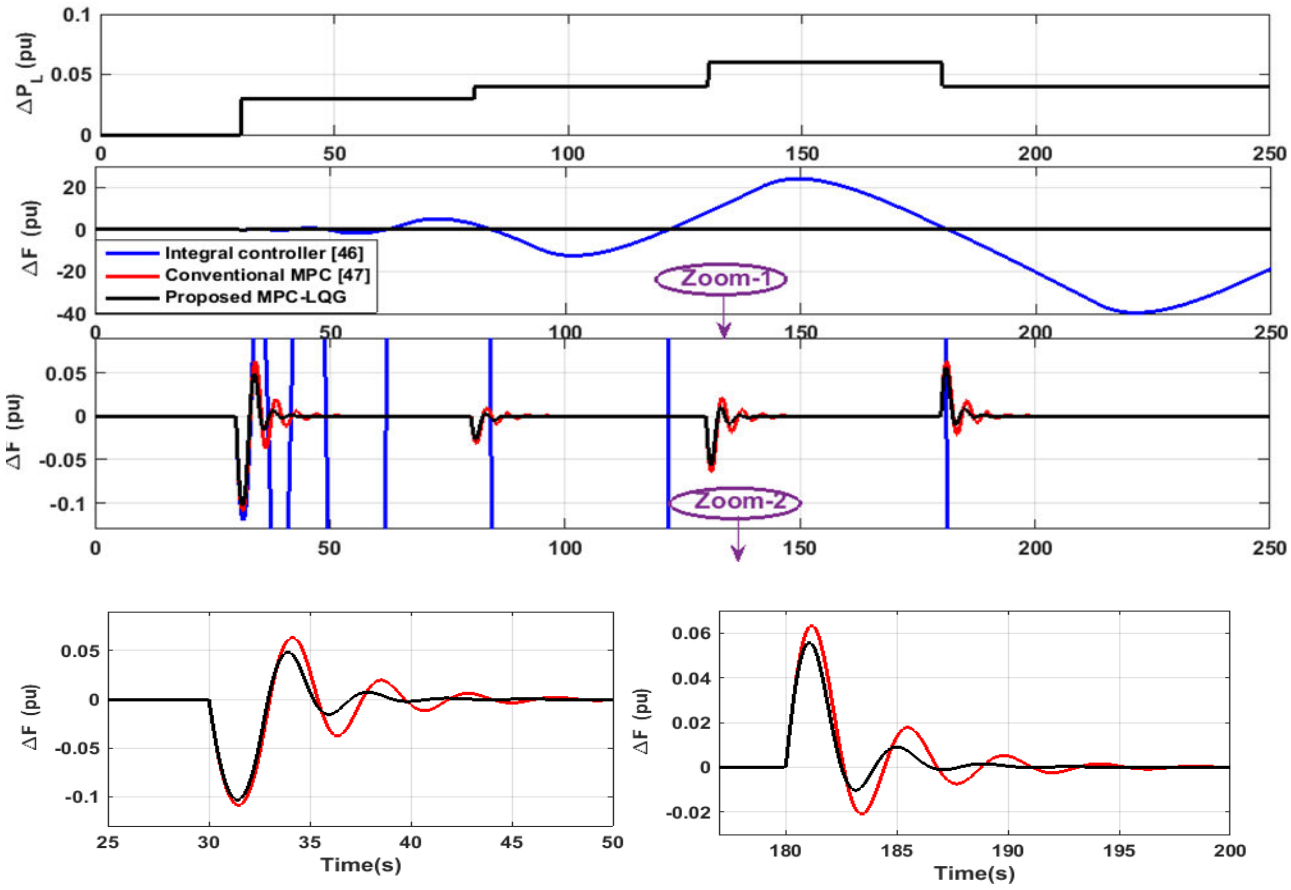

FIGURE 16. The single-area power system performance relied on various control techniques for case A, scenario 3.

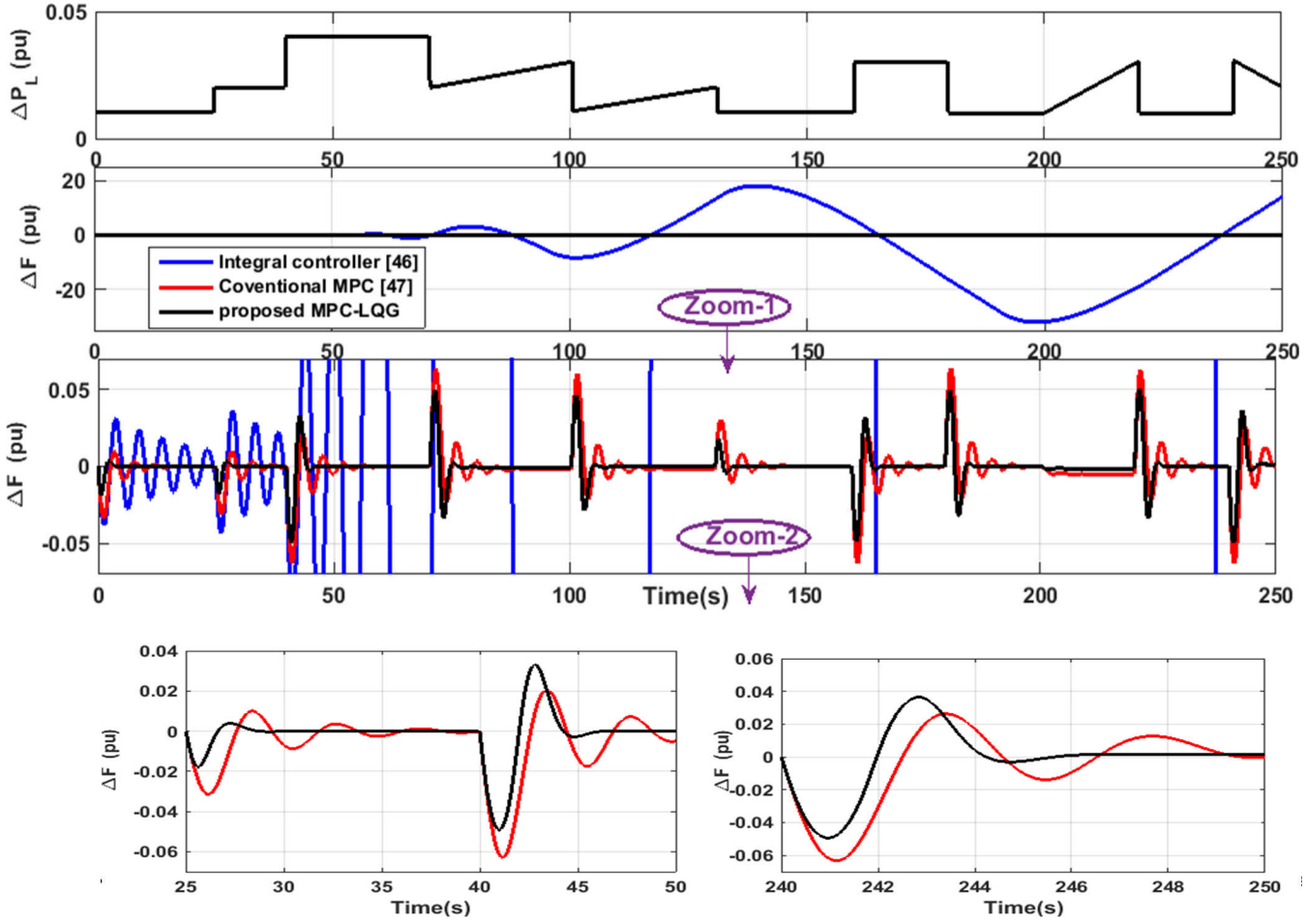

FIGURE 17. The single-area power system performance relied on various control techniques for case B, scenario 3.

are connected to the considered system at time t = 50 sec, and t = 500 sec respectively. Furthermore, Figure 19 displays the studied system performance based on the MPC-LQG controller relied on ChOA algorithm considering different penetrations of the wind power (i.e. 3% penetration and 6% penetration). From the simulation results, the MPC-LQG controller improves the system stability in face of the resulted oscillations from the wind power as well as load disturbances. The system performance specifications are within the range of acceptance.

Case B: in this case, the performance of the system under consideration is tested and evaluated considering variations in the system bounds as well as the interpenetrating of the wind power, and a random load disturbance. Figure 20 displays the performance of the system based on the proposed controller considering different levels of wind power penetration. It is clear from Figure 20 that the proposed controller still able to keep the system stable under all considered disturbances. These results address the ability of the proposed MPC–LQG controller relied on the ChOA technique for dealing with the effect of the high renewables penetration, system uncertainties, and nonlinearities.

E. SCENARIO 5. PERFORMANCE EVALUATION OF MULTI-AREA INTERCONNECTED POWER SYSTEM

In this scenario, the proposed MPC-LQG controller is applied to a two-area interconnected power system considering system nonlinearities as shown in Figure 21. The rated power capacity of area-1 is 2000 MVA and the rated power capacity of area-2 is 2250 MVA. Also, the studied system parameters are listed in Table 9. While Table 10 shows the optimal parameters of the proposed MPC-LQG controllers, which are designed for each area of the studied two-area interconnected power system. Furthermore, this scenario is divided into two sections.

Case A: This case clarifies the estimation of the system performance based on the proposed controller and other controllers (e.g. integral controller [46], the conventional MPC [30]) under the system's normal parameters, and applying a 2% step load change at area-2 for the considered system at t = 3 sec. Figure 22 shows the response of the studied two-area interconnected power system with the proposed robust MPC-LQG controller and other conventional controllers. Where, the frequency deviations of the studied

TABLE 8. The optimum constraints of the proposed MPC-LQG based ChOA considering wind power penetration.

optimization	Ts	P	M	R_{MPC}	Q_{MPC}	K_L	K_Q	K_R
ChOA	0.1043	2.4971	1.6742	1	10	0.0015	-0.0733	-0.0295

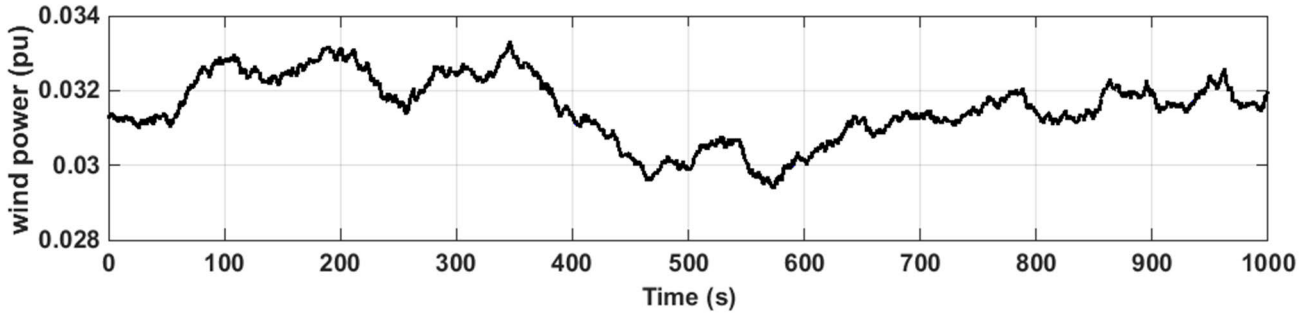

FIGURE 18. The wind power variations.

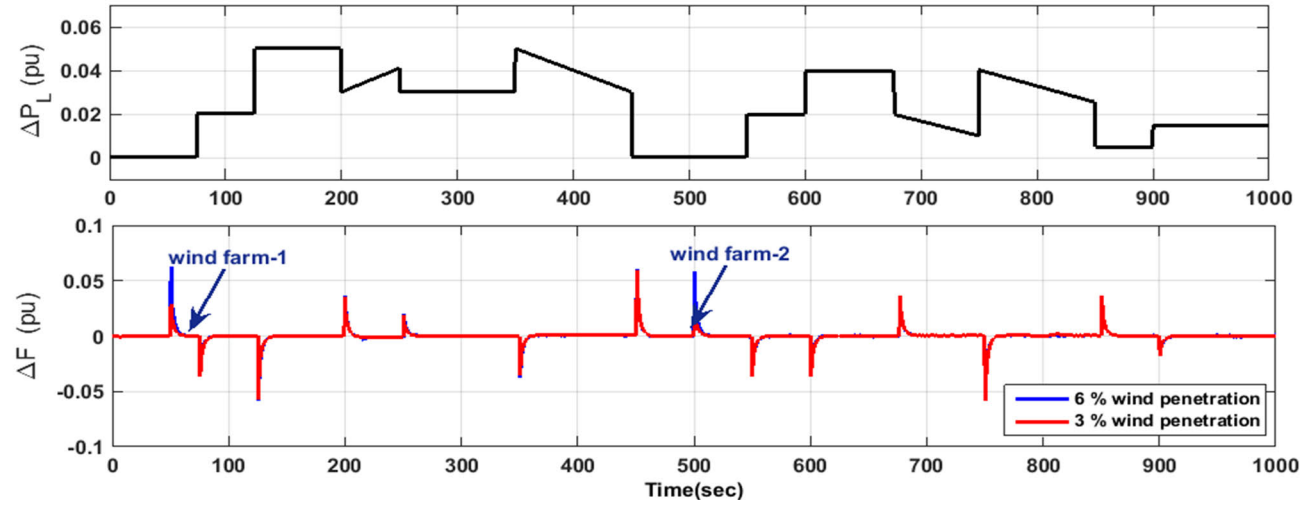

FIGURE 19. The single-area power system performance relied on the proposed controller reputing different wind power interpenetrating for case A, scenario 4.

system with the integral controller is about ±0.06 Hz for area 1 and ±0.048 Hz for area 2, while the conventional MPC controller gives a frequency deviation in a range of ±0.057 Hz for area 1 and ±0.0047 Hz for area 2. On the other hand, the frequency deviations of the studied two-area interconnected power system with the proposed robust controller is about ±0.04 Hz for area 1 and ±0.03 Hz for area 2. It is worth noting that the system performance based on the proposed MPC-LQG controller based on the ChOA algorithm is more stable and fast at achieving stability. While the performance of the system based on the conventional integral controller is seriously degraded.

Case B: In this case, the efficacy of the proposed MPC-LQG controller based on the ChOA algorithm is checked and evaluated, considering wind power penetration. As illustrated in Figure 20, a wind power source-1 has been linked to area-1 at t = 200 sec, a wind power source-2 at t = 600 sec, and a 2% step load change has been applied to area-2 at t = 30 sec in the considered system. Figure 18 prominently

TABLE 9. Parameters for the two-area power system under analysis.

Parameters	Area-1	Area-2
D (pu.MW/Hz)	0.015	0.016
H (pu. MW s)	0.0833	0.1008
T_g (sec)	0.08	0.06
T_t (sec)	0.4	0.44
R (Hz/ pu.MW)	3	2.73
GRC (pu.MW / minute)	10%	10%
GDB (Hz)	0.006	0.006
K_i	-0.3	-0.2
T_{12}	0.2	

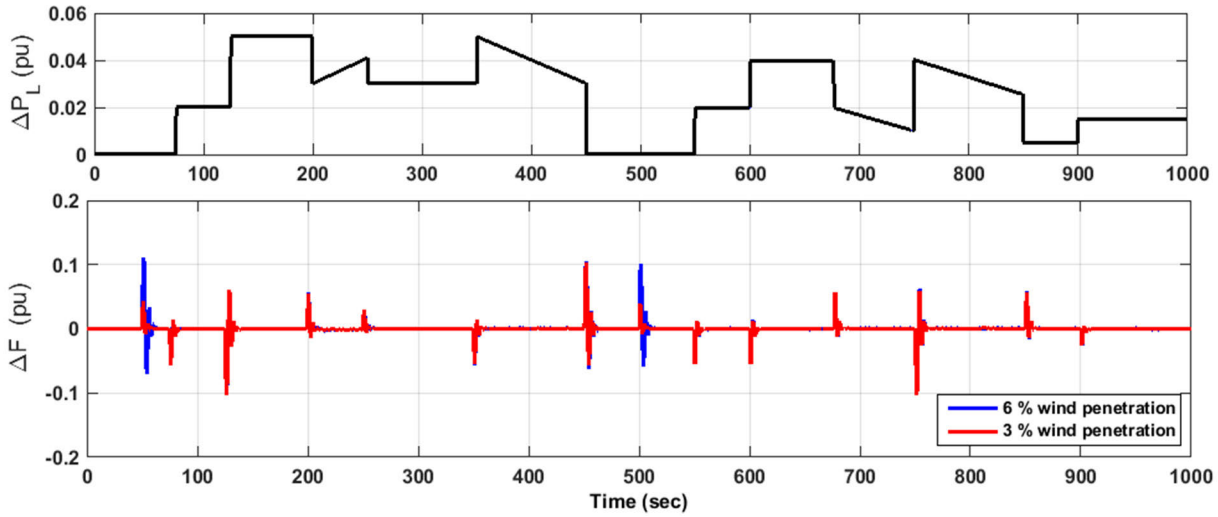

FIGURE 20. The single-area power system performance relied on the proposed controller reputing different wind power interpenetrating for case B, scenario 4.

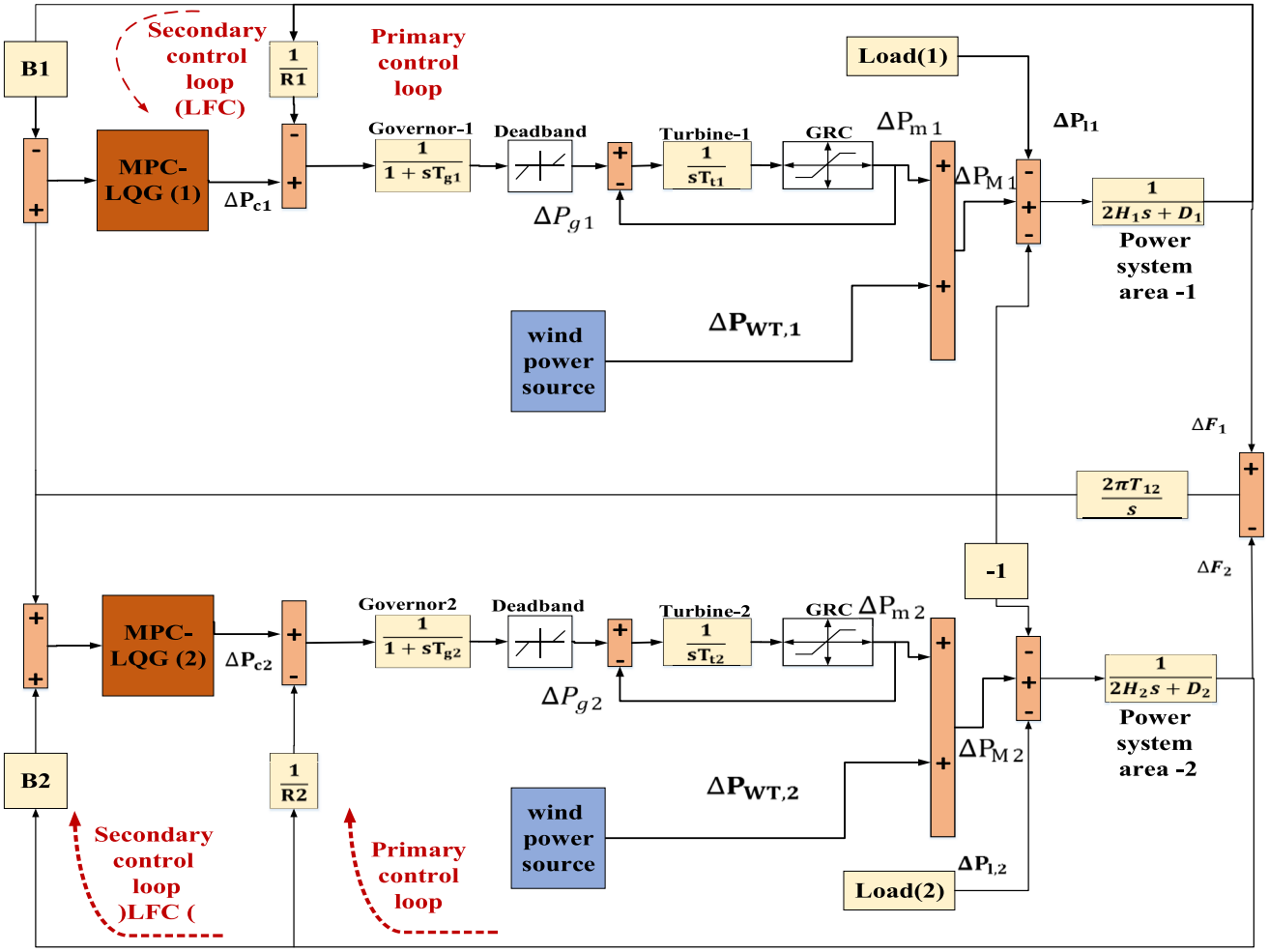

FIGURE 21. The block diagram of the considered two-area interconnected power system.

displays the output of the wind power source. Furthermore, Figure 23 displays the performance of the studied system based on the proposed controller considering wind power penetration in each area of the considered system. The proposed MPC-LQG controller maintains system stability in the face of wind power penetration and load disturbances.

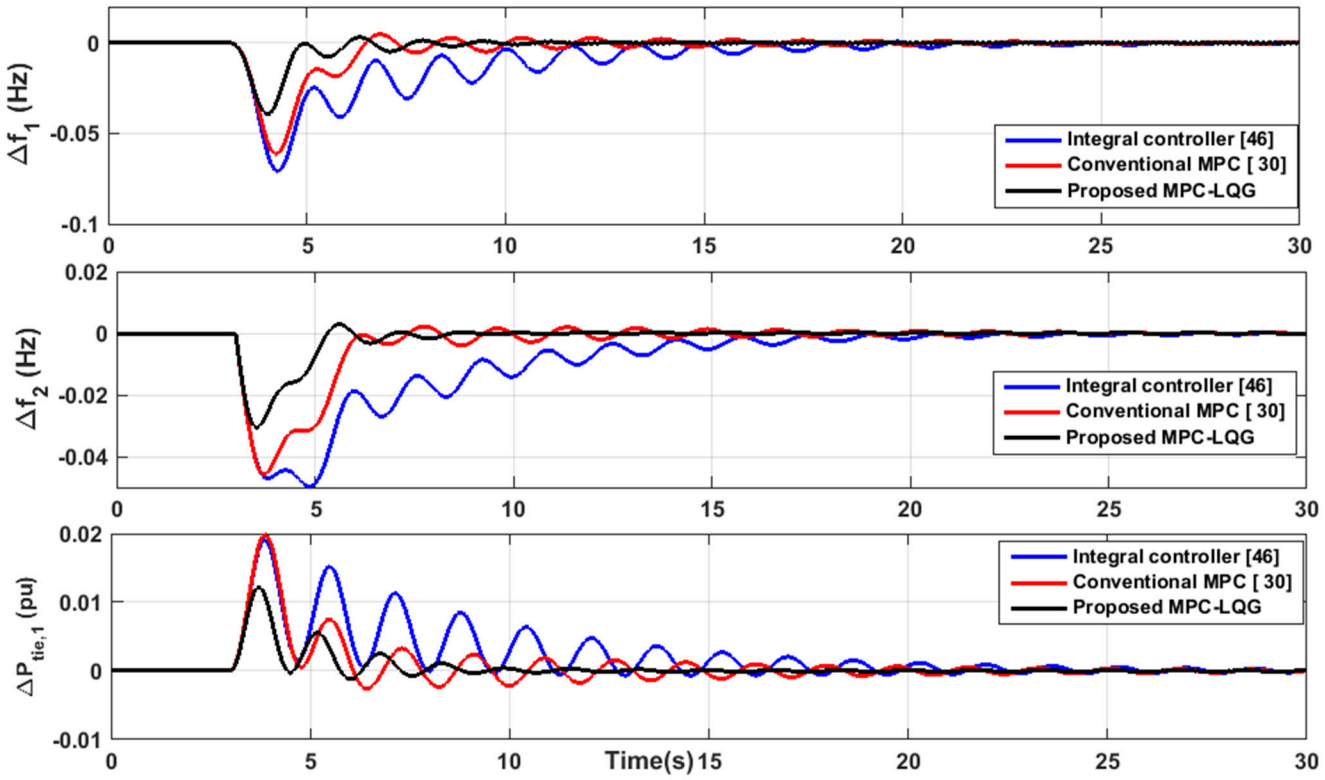

FIGURE 22. The two-area system performance relied on the proposed controller for case A, scenario 5.

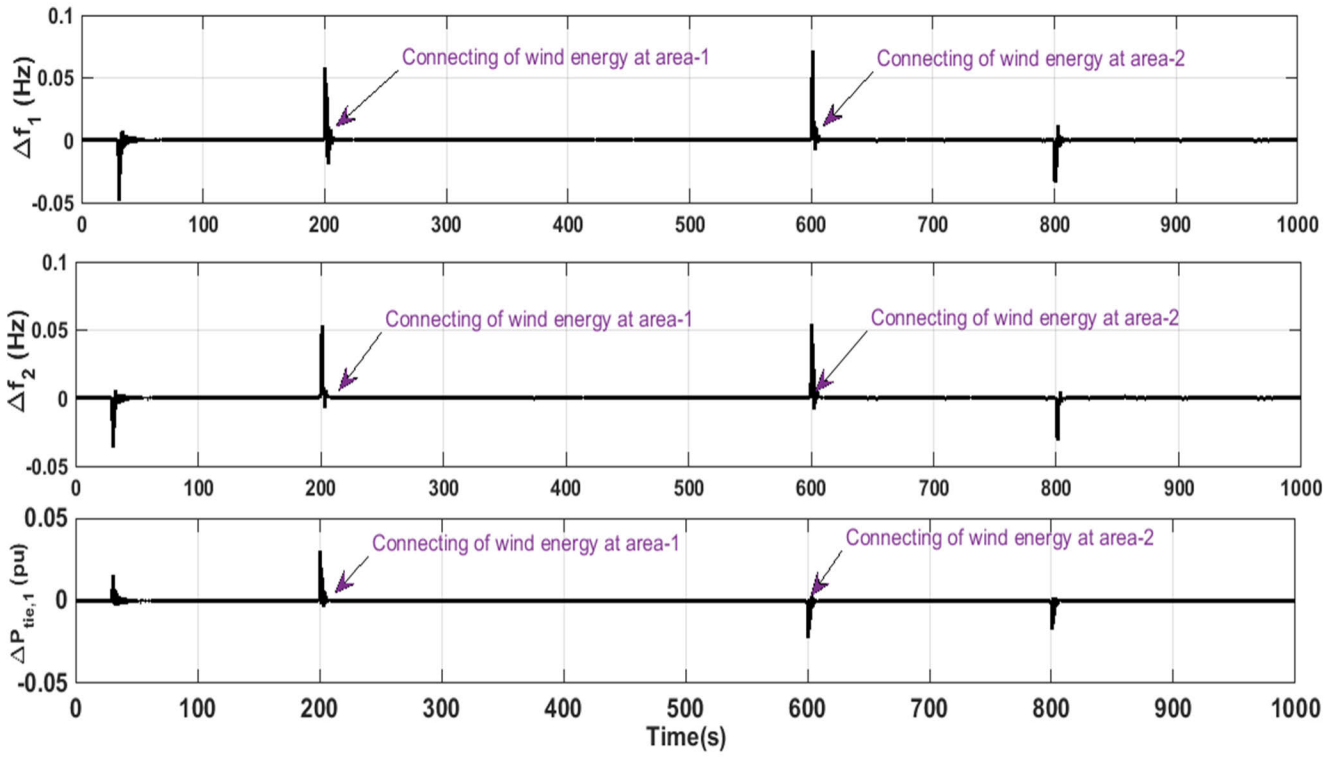

FIGURE 23. The two-area system performance relied on the proposed controller reputing wind power interpenetrating for case B, scenario 5.

TABLE 10. The parameters of the designed controllers; proposed controller, integral controller, and conventional MPC controller for the studied two-area power system.

Controller	Area-1	Area-2
The integral controller [46]	$k_i = -0.3$	$k_i = -0.2$
The conventional MPC [30]	P=13 , M=2 , T_s=0.0002 ,Weights on manipulated variables = 0 ,Weights on manipulated variable rates = 0.1 ,Weights on the output signals = 1, max control action = 0.25 pu, min control action =-0.25 pu, max frequency deviation = 1 pu, min frequency deviation =-1 pu	
The proposed MPC–LQG controller	P=20 , M=2.2666 , T_s=0.0182, R_{MPC}= 1, Q_{MPC}= 5.3681 , K_l= 0.0099 , K_q= 0.0607, K_r= 0.0121, K_{rg}= -0.0680	P=2.2710 , M=3.1132 , T_s=0.1270, R_{MPC}= 1.7835 , Q_{MPC}= 8.7273 , K_l= 0.0720 , K_q= 0.3019 , K_r= 0.0590, K_{rg}= -0.2956

VI. CONCLUSION

The main points of this article can be summarized as follows:

- A robust MPC-LQG controller has been proposed to eliminate the system fluctuations resulting from system nonlinearities, uncertainties, and high wind power penetration.
- The parameters of the proposed MPC-LQG controller have been estimated by a novel algorithm known as ChOA algorithm due to its merits (i.e. fast convergence speed, good exploration, and exploitation).
- More than scenarios were run to test the robustness of the proposed controller.
- The simulation outcomes proved that the proposed MPC-LQG controller enhances the frequency stability under all considered scenarios (i.e. different patterns of loads, system parameters variations, and high wind power penetration).
- The proposed control strategy enhances the system performance better than the integral controller by 33 percentage.
- The proposed control strategy enhances the system performs better than the conventional MPC controller by 22 percentage
- Briefly, the proposed MPC-LQG controller can be applied to modern power grids.

Some points will be considered for future work and can be summarized as follows:

- Applying several renewable energy sources with different levels of penetration as well as different types of energy storage systems to upgrade the existing power systems toward modern renewable power systems.
- Applying new optimization algorithms and their proposed modifications to select the optimal parameters of the considered frequency controller under different operating conditions.
- Applying different control strategies like (i.e. cascaded control strategy, feedback- feed-forward control strategy – hybrid control strategy) to enhance the frequency stability.
- Applying voltage regulation control to the considered system to control the frequency and voltage at the same time.

ACKNOWLEDGMENT

This work was supported by the National Research and Development Agency of Chile (ANID) under Grant ANID/Fondap/15110019.

REFERENCES

[1] O. Aissa, S. Moulahoum, I. Colak, B. Babes, and N. Kabache, "Analysis and experimental evaluation of shunt active power filter for power quality improvement based on predictive direct power control," *Environ. Sci. Pollut. Res.*, vol. 25, no. 25, pp. 24548–24560, 2017.

[2] A. Abazari, M. M. Soleymani, M. Babaei, M. Ghafouri, H. Monsef, and M. T. H. Beheshti, "High penetrated renewable energy sources-based AOMPC for microgrid's frequency regulation during weather changes, time-varying parameters and generation unit collapse," *IET Gener., Transmiss. Distrib.*, vol. 14, no. 22, pp. 5164–5182, Nov. 2020.

[3] N. Hamouda, B. Babes, S. Kahla, Y. Soufi, J. Petzoldt, and T. Ellinger, "Predictive control of a grid connected PV system incorporating active power filter functionalities," in *Proc. 1st Int. Conf. Sustain. Renew. Energy Syst. Appl. (ICSRESA)*, Dec. 2019, pp. 1–6.

[4] M. Khamies, G. Magdy, M. E. Hussein, F. A. Banakhr, and S. Kamel, "An efficient control strategy for enhancing frequency stability of multi-area power system considering high wind energy penetration," *IEEE Access*, vol. 8, pp. 140062–140078, 2020.

[5] B. E. Sedhom, M. M. El-Saadawi, M. A. Elhosseini, M. A. Saeed, and E. E. Abd-Raboh, "A harmony search-based H-infinity control method for islanded microgrid," *ISA Trans.*, vol. 99, pp. 252–269, Apr. 2020.

[6] H. Ali, G. Magdy, B. Li, G. Shabib, A. A. Elbaset, D. Xu, and Y. Mitani, "A new frequency control strategy in an islanded microgrid using virtual inertia control-based coefficient diagram method," *IEEE Access*, vol. 7, pp. 16979–16990, 2019.

[7] H. Bevrani, M. R. Feizi, and S. Ataee, "Robust frequency control in an islanded microgrid: H_∞ and μ-synthesis approaches," *IEEE Trans. Smart Grid*, vol. 7, no. 2, pp. 706–717, Mar. 2016.

[8] M. Khan, H. Sun, Y. Xiang, and D. Shi, "Electric vehicles participation in load frequency control based on mixed H_2/H_∞," *Int. J. Electr. Power Energy Syst.*, vol. 125, Feb. 2021, Art. no. 106420.

[9] P. Moniya and B. Anand, "Automatic generation control with fuzzy logic controller incorporating tandem and cross compound turbine," *J. Ambient Intell. Humanized Comput.*, vol. 12, no. 7, pp. 7071–7083, Jul. 2021.

[10] M. U. Jan, A. Xin, M. A. Abdelbaky, H. U. Rehman, and S. Iqbal, "Adaptive and fuzzy PI controllers design for frequency regulation of isolated microgrid integrated with electric vehicles," *IEEE Access*, vol. 8, pp. 87621–87632, 2020.

[11] H. Yousef, "Adaptive fuzzy logic load frequency control of multi-area power system," *Int. J. Electr. Power Energy Syst.*, vol. 68, pp. 384–395, Jun. 2015.

[12] S. K. Akula and H. Salehfar, "Frequency control in microgrid communities using neural networks," in *Proc. North Amer. Power Symp. (NAPS)*, Wichita, KS, USA, Oct. 2019, pp. 1–6.

[13] G. Sharma, A. Panwar, Y. Arya, and M. Kumawat, "Integrating layered recurrent ANN with robust control strategy for diverse operating conditions of AGC of the power system," *IET Gener., Transmiss. Distrib.*, vol. 14, no. 18, pp. 3886–3895, Sep. 2020.

[14] G. Magdy, G. Shabib, A. A. Elbaset, T. Kerdphol, Y. Qudaih, H. Bevrani, and Y. Mitani, "Tustin's technique based digital decentralized load frequency control in a realistic multi power system considering wind farms and communications delays," *Ain Shams Eng. J.*, vol. 10, no. 2, pp. 327–341, Jun. 2019.
[15] X. Shang-Guan, Y. He, C. Zhang, L. Jiang, J. W. Spencer, and M. Wu, "Sampled-data based discrete and fast load frequency control for power systems with wind power," *Appl. Energy*, vol. 259, Feb. 2020, Art. no. 114202.
[16] S. K. Das, M. Rahman, S. K. Paul, M. Armin, P. N. Roy, and N. Paul, "High-performance robust controller design of plug-in hybrid electric vehicle for frequency regulation of smart grid using linear matrix inequality approach," *IEEE Access*, vol. 7, pp. 116911–116924, 2019.
[17] M. Rahman, S. K. Sarkar, S. K. Das, and Y. Miao, "A comparative study of LQR, LQG, and integral LQG controller for frequency control of interconnected smart grid," in *Proc. 3rd Int. Conf. Electr. Inf. Commun. Technol. (EICT)*, Khulna, Bangladesh, Dec. 2017, pp. 1–6.
[18] G. Magdy, G. Shabib, A. A. Elbaset, T. Kerdphol, Y. Qudaih, and Y. Mitani, "A novel design of decentralized LFC to enhance frequency stability of Egypt power system including wind farms," *Int. J. Energy Convers.*, vol. 6, no. 1, p. 17, Jan. 2018.
[19] Y.-H. Moon, H.-S. Ryu, B. Kim, and K.-B. Song, "Optimal tracking approach to load frequency control in power systems," in *Proc. IEEE Power Eng. Soc. Winter Meeting. Conf.*, Singapore, Jan. 2000, pp. 1371–1376.
[20] M. Aoki, "Control of large-scale dynamic systems by aggregation," *IEEE Trans. Autom. Control*, vol. AC-13, no. 3, pp. 246–253, Jun. 1968.
[21] P. N. Topno and S. Chanana, "Load frequency control of a two-area multi-source power system using a tilt integral derivative controller," *J. Vib. Control*, vol. 24, no. 1, pp. 110–125, Jan. 2018.
[22] H. M. Hasanien and A. El-Fergany, "Salp swarm algorithm-based optimal load frequency control of hybrid renewable power systems with communication delay and excitation cross-coupling effect," *Electr. Power Syst. Res.*, vol. 176, pp. 1–10, Nov. 2019.
[23] G. Magdy, E. A. Mohamed, G. Shabib, A. A. Elbaset, and Y. Mitani, "SMES based a new PID controller for frequency stability of a real hybrid power system considering high wind power penetration," *IET Renew. Power Gener.*, vol. 12, no. 11, pp. 1304–1313, 2018.
[24] Y. Arya, P. Dahiya, E. Çelik, G. Sharma, H. Gözde, and I. Nasiruddin, "AGC performance amelioration in multi-area interconnected thermal and thermal-hydro-gas power systems using a novel controller," *Eng. Sci. Technol., Int. J.*, vol. 24, no. 2, pp. 384–396, Apr. 2021.
[25] S. M. Nosratabadi, M. Bornapour, and M. A. Gharaei, "Grasshopper optimization algorithm for optimal load frequency control considering predictive functional modified PID controller in restructured multi-resource multi-area power system with redox flow battery units," *Control Eng. Pract.*, vol. 89, pp. 204–227, Aug. 2019.
[26] M. Elsisi, "New variable structure control based on different meta-heuristics algorithms for frequency regulation considering nonlinearities effects," *Int. Trans. Electr. Energ. Syst.*, vol. 30, no. 7, p. e12428, 2020.
[27] N. Kumar, B. Tyagi, and V. Kumar, "Application of fractional order PID controller for AGC under deregulated environment," *Int. J. Autom. Comput.*, vol. 15, no. 1, pp. 84–93, Feb. 2018.
[28] A. N. Venkat, I. A. Hiskens, J. B. Rawlings, and S. J. Wright, "Distributed MPC strategies with application to power system automatic generation control," *IEEE Trans. Control Syst. Technol.*, vol. 16, no. 6, pp. 1192–1206, Nov. 2008.
[29] T. H. Mohamed, G. Shabib, E. H. Abdelhameed, M. Khamies, and Y. Qudaih, "Load frequency control in single area system using model predictive control and linear quadratic Gaussian techniques," *Int. J. Electr. Energy*, vol. 3, no. 3, pp. 141–144, 2015.
[30] T. H. Mohamed, H. Bevrani, A. A. Hassan, and T. Hiyama, "Decentralized model predictive based load frequency control in an interconnected power system," *Energy Convers. Manage.*, vol. 52, no. 2, pp. 1208–1214, 2011.
[31] G. Magdy, G. Shabib, A. A. Elbaset, and Y. Mitani, "Frequency stabilization of renewable power systems based on MPC with application to the Egyptian grid," *IFAC-PapersOnLine*, vol. 51, no. 28, pp. 280–285, 2018.
[32] J. Liu, Q. Yao, and Y. Hu, "Model predictive control for load frequency of hybrid power system with wind power and thermal power," *Energy*, vol. 172, pp. 555–565, Apr. 2019.
[33] T. H. Mohamed, J. Morel, H. Bevrani, and T. Hiyama, "Model predictive based load frequency control_design concerning wind turbines," *Int. J. Electr. Power Energy Syst.*, vol. 43, no. 1, pp. 859–867, Dec. 2012.
[34] M. U. Jan, A. Xin, H. U. Rehman, M. A. Abdelbaky, S. Iqbal, and M. Aurangzeb, "Frequency regulation of an isolated microgrid with electric vehicles and energy storage system integration using adaptive and model predictive controllers," *IEEE Access*, vol. 9, pp. 14958–14970, 2021.
[35] M. A. Mohamed, A. A. Z. Diab, H. Rezk, and T. Jin, "A novel adaptive model predictive controller for load frequency control of power systems integrated with DFIG wind turbines," *Neural Comput. Appl.*, vol. 32, no. 11, pp. 7171–7181, Jun. 2020.
[36] X. Shi, G. Wen, J. Cao, and X. Yu, "Model predictive power dispatch and control with price-elastic load in energy internet," *IEEE Trans. Ind. Informat.*, vol. 15, no. 3, pp. 1775–1787, Mar. 2019.
[37] G. Wen, G. Hu, J. Hu, X. Shi, and G. Chen, "Frequency regulation of source-grid-load systems: A compound control strategy," *IEEE Trans. Ind. Informat.*, vol. 12, no. 1, pp. 69–78, Feb. 2016.
[38] N. Hamouda, B. Babes, S. Kahla, and Y. Soufi, "Real time implementation of grid connected wind energy systems: Predictive current controller," in *Proc. 1st Int. Conf. Sustain. Renew. Energy Syst. Appl. (ICSRESA)*, Dec. 2019, pp. 1–6.
[39] M. Elsisi, M. Soliman, M. A. S. Aboelela, and W. Mansour, "Bat inspired algorithm based optimal design of model predictive load frequency control," *Int. J. Electr. Power Energy Syst.*, vol. 83, pp. 426–433, Dec. 2016.
[40] M. Elsisi, M. Aboelela, M. Soliman, and W. Mansour, "Design of optimal model predictive controller for LFC of nonlinear multi-area power system with energy storage devices," *Electr. Power Compon. Syst.*, vol. 46, nos. 11–12, pp. 1300–1311, Jul. 2018.
[41] M. Elsisi, "New design of adaptive model predictive control for energy conversion system with wind torque effect," *J. Cleaner Prod.*, vol. 240, Dec. 2019, Art. no. 118265.
[42] H. H. Ali, A. Fathy, and A. M. Kassem, "Optimal model predictive control for LFC of multi-interconnected plants comprising renewable energy sources based on recent sooty terns approach," *Sustain. Energy Technol. Assessments*, vol. 42, Dec. 2020, Art. no. 100844.
[43] S. H. Shahalami and D. Farsi, "Analysis of load frequency control in a restructured multi-area power system with the Kalman filter and the LQR controller," *AEU-Int. J. Electron. Commun.*, vol. 86, pp. 25–46, Mar. 2018.
[44] M. Khamies, G. Magdy, M. Ebeed, and S. Kamel, "A robust PID controller based on linear quadratic Gaussian approach for improving frequency stability of power systems considering renewables," *ISA Trans.*, Jan. 2021, doi: 10.1016/j.isatra.2021.01.052.
[45] M. Khishe and M. R. Mosavi, "Chimp optimization algorithm," *Expert Syst. Appl.*, vol. 149, Jul. 2020, Art. no. 113338.
[46] H. Bevrani, *Robust Power System Control*. New York, NY, USA: Springer, 2009.
[47] T. H. Mohamed, A. A. Hassan, H. Bevrani, and T. Hiyama, "Model predictive based load frequency control design," in *Proc. 16th Int. Conf. Elect. Eng.*, Busan, South Korea, Jul. 2010, pp. 1–6.
[48] M. A. El-Hameed and A. A. El-Fergany, "Water cycle algorithm-based load frequency controller for interconnected power systems comprising non-linearity," *IET Gener., Transmiss. Distrib.*, vol. 10, no. 15, pp. 3950–3961, Nov. 2016.
[49] J. G. Van Antwerp and R. D. Braatz, "A tutorial on linear and bilinear matrix inequalities," *J. Process Control*, vol. 10, no. 4, pp. 363–385, 2000.